# SCALING AND UNCERTAINTY IN LANDSAT REMOTE SENSING OF BIOPHYSICAL ATTRIBUTES

by

Aiden Vincent Johnson

A thesis submitted in partial fulfillment
of the requirements for the degree

of

Master of Science

in

Land Resources and Environmental Sciences

MONTANA STATE UNIVERSITY
Bozeman, Montana

January 2015

# ACKNOWLEDGEMENTS

I would like to thank my academic advisor Dr. Paul Stoy for his research guidance and unwavering excitement for advancing science and performing research. In addition, I would like to extend my gratitude to the members of my academic committee: Dr. Scott Powell, Dr. Stephanie Ewing, Dr. Mark Greenwood, and Dr. Nate Brunsell. Without their collective knowledge, support, and patience, this research would not have been possible. The knowledge and academic development provided by my course work at Montana State University is also a significant contribution to the completion of not only this research, but my intellectual and personal development. Many fellow graduate students played an important role in this research as well including: Adam Sigler, Liza Harris, Angela Tang, Aaron Rains, Chris Welch, Carmel Johnston, Christine Miller, Byran Amerson, Sam Carlson, and Patrick Lawrence. Individuals who provided notable academic guidance and professional support include: Dr. Dan Goodman, Dr. Lucy Marshall, Dr. Tony Hartshorn, and Dr. Paul Hook.

Finally, I would like to thank my friends and family for their love and support. I would especially like to thank my parents for their endless encouragement of my perpetually changing pursuits and my fiancé Krista Ehlert for her grounding perspective.

TABLE OF CONTENTS

TABLE OF CONTENTS - CONTINUED

# LIST OF TABLES

# LIST OF FIGURES

LIST OF FIGURES – CONTINUED

Figure Page

# ABSTRACT

Monitoring environmental change is of high importance in our time of global change. Remote sensing technology provides the tools to view the ecological dynamics at a landscape scale and review the change through time with time series data availability. Creating congruence between data scales and functional scales is a long standing challenge for Earth system scientists. In this research we evaluate methods for change detection and scaling data in a discontinuous permafrost zone of central Alaska and is characterized by pronounced permafrost thaw and methane release over decadal to century timescales. The primary goal is to evaluate the applicability of Landsat satellite remote sensing for detecting bog thermal expansion over time. We implement a Random Forests classification scheme in order to separate the landscape into its various land features and bog types, many features in this landscape are developed through an aged-stage transition of thermal expansion. The results of this classification were dominated by hydrologic features, with a 0.05 increase in mean albedo, providing essentially no change in both mean Normalized Difference Vegetation Index (NDVI) and mean Brightness Temperature (BT). In addition, we attempt to capture the scales of variation within the landscape using multi-resolution methods. The scale of variance as illustrated by a wavelet analysis for NDVI show the greatest amount of variance around 4.5 km to 5 km. Brightness Temperature had three peaks of high variance between 0.06 km - 1 km including maximum variance at about 0.5 km and a pair of peaks between 3 km and 4 km. An important component of any data analysis is quantifying the uncertainty. Uncertainty quantification in remote sensing data analysis is often over looked. In a second analysis we attempt to quantify the primary sources of uncertainty in Landsat remote sensing data via simulation methods. Specifically, we evaluate the level of uncertainty contributed to the data by applying a typical atmospheric correction through Monte Carlo simulation approach to estimate the total variance within several Landsat scenes. We find the contribution of uncertainty due to the MODTRAN conversion to be between 7-27% differing by total scene variance per image.

# CHAPTER ONE

# INTRODUCTION

## Terrestrial Satellite Remote Sensing

Earth observing satellites have been an integral part of ecological studies across the globe for nearly 40 years. Beginning in the 1970's with the launch of the Landsat 1 by NASA and followed by many other nations across the globe, coordinated efforts were launched to develop a succinct and complete record of as much of the earth surface as possible (Lillesand & Kiefer, 2004). This contributed immensely to our understanding of global water and energy cycles. As well as providing views of land cover and land cover change at the landscape scale.

Water resources monitoring have been hugely influenced by satellite remote studies. Glaciers, seasonal fluctuations in stream flow through out watersheds, snowpack, and vegetation and soil interactions. Sediment transport is an important hydrologic concern in which remote sensing has been explored as tool for monitoring (Stumpf & Pennock, 1989).

Forest inventory and monitoring has expanded and improved in accuracy by the use of remotely sensed vegetation maps, classification sometimes down to species level has improved regional forest management tremendously, through habitat composition studies, biodiversity and resiliency studies and recreational studies (Hyyppä, J., Hyyppä, H., Inkinen, Engdahl, Linko, & Zhu, 1998). Similarly, agricultural resources have been increasingly monitored via remote sensing methods (Long, 2014)

## Landsat Satellites

Landsat 5 TM launched in March of 1984 was one of the longest functioning earth observing satellites in existence (Markham, Storey, Williams, & Irons, 2004). Most contemporary scientific research involving Landsat data incorporates data from either one or several of the following Landsat 5 TM, 7 ETM +, and 8 TIRS; Landsat 6 failed to reach orbit. All Landsat satellites are passive, the energy they sense is from the sun and it was reflected by the target's surface, subsequently the satellite's orbits are all sun synchronous.

## Change Detection

Methods of change detection that inform scientists' ability to understand mechanisms of change and ecological trajectories or transitions have been a major part of the development of terrestrial remote sensing as a scientists toolbox. Land use and Land cover change are an integral part of remote sensing studies. This has become a key component of satellite remote sensing with the advent of ever improving computational power and data storage capacities. The depth of the temporal data record and the continued evolution of processing algorithms have led to year by year change detection products such as Vegetation Change Tracker (Huang., Goward, Masek, Gao, Vermote, Thomas, & Townshend, 2009) showing spatially explicit forest disturbance and reforestation. Other example methods for change detection include: time series analysis, trend analysis, piece-wise regression, classification and image differencing or image subtraction.

## Scale as a Term

Dimensions of scale can be spatial or temporal and often the case is both. Variations of ecological processes, which are not cyclic in nature, across multiple scales and dimensions, are often the focus of earth system studies (Meentenmeyer & Box, 1987). Process scale is the scale at which an earth system process occurs or the scale of the event or phenomenon of interest. Unfortunately, often times the process scale is different than the observation scale with which we can observe some phenomenon within an ecosystem. Observational scale is the scale by which we can measure and record some part of an earth system process.

Often the mismatch between the process or intrinsic scale and the observational scale creates difficulties for monitoring phenomena of interest.

## Scaling in Landsat Remote Sensing Ecological Studies

Scaling up and scaling down are inevitable topics in satellite remote sensing analysis due to its spatial nature. Effective scaling requires quantifying the variance or the probability associated with certain values occurring in the data in order to transfer that data to a different spatial scale (Fisher, Mustard, & Vadeboncoeur, 2006). Scaling within the temporal dimension is also an important topic for substituting the temporal for spatial dimension studies. Multi-resolution methods are appropriate for quantifying scales of variance and allow for temporal change detection and detail analysis (Hu & Islam, 1997).

## Multi-Resolution Methods for Scaling Problems

Solutions for addressing scaling problems come from many different disciplines outside of ecology, including digital signal processing. Some examples of methods that have been implemented to deal with scaling translations include: Spectral analysis, fractals, Wavelets, geostatistics, and multi-scale object oriented analysis. Spectral analysis uses fits of sines and cosines on density data to evaluate periodicity (Ripley 1978). Fractals are a more recently applied method based on a continuous or fractional dimension rather than an integer function. Wavelets analysis is very similar to spectral analysis except the fit is to a wavelet function rather than a sine, cosine as a basis system. Geostatistics is a branch of statistics focused on estimating models associated with spatial and/or temporal locations. Multi-scale object oriented analysis is the grouping of similar groups of data into discrete regions based on similarity and of potentially different sized clusters depending on scale and similarity of data in clusters.

## Motivation for Scaling Change Detection (Ch. 2)

Arctic and subarctic systems have experienced substantial warming over the past century ( Chapin, Sturm, Serreze, McFadden, Key, Lloyd, & Welker, 2005; Moritz, Bitz, & Steig, 2002), which has led to shifts in vegetation cover such as shrub encroachment (Forbes, Fauria, & Zetterberg, 2010). Arctic and subarctic systems tend to be highly heterogeneous at spatial scales far smaller than commonly-used remote sensing platforms such as MODIS (Asner, Scurlock, & Hicke, 2003). To understand vegetation change in

high-latitude ecosystems, we need to quantify the spatial scales at which these changes are occurring.

## Uncertainty in Terrestrial Remote Sensing

The practice of reporting uncertainty in biophysical uses of Landsat satellite data derivatives is not commonplace. Landsat imagery has been widely used for remote sensing applications in ecology. Despite the wide applicability of Landsat imagery (Roy, 2014), insufficient work has assessed the uncertainty of Landsat data and its associated biophysical products. In remote sensing data analysis, estimates of variance usually consist of an accuracy assessment of a classification product and fail to evaluate the sources of error going into the classification such as parameters incorporated in estimating land surface temperature. Those unreported levels of uncertainty are often then fed into an ecosystem model to address a question, resulting in an unknown confidence in the product of the ecosystem model.

## Typical Uncertainty Analysis of Remote Sensing Data

Often an analysis used to evaluate the performance of a model are comparisons of different models outcomes for some biophysical attribute. For example, much of the work done to evaluate different Global Circulation Models (GCM) is centered on how each models climate predictions differ from the other without discussing much about the uncertainty inherent in the model method or the data incorporated (Turner, Ritts, Cohen, Maeirsperger, Gower, Kirschbaum, Running, Zhao, Wofsy, Dunn, Law, Campbell,

Oechel, Kwon, Meyers, Small, Kurc, and Gamon, 2005). These studies are important for choosing an appropriate model for your particular research scenario. Yet these model comparisons do not inform our confidence in the model products. In remote sensing studies it is often the case that different classification techniques are compared and the comparisons are based on evaluating accuracy of land classification product as compared to its in situ land class. This type of analysis informs ones choices in terms of a classifier, but doesn't include information about accuracy of biophysical attributes derived from remote sensing. Comparing biophysical attributes derived from different remote sensing sensors (Ferguson, Sheffield, Wood, & Gao, 2010) is another method for evaluating uncertainty that is no different than comparing different ecological models.

These model comparisons inform the user about certain model and data appropriateness; however, they fail address the uncertainty attributed to an estimate of an individual model and to identify what the primary source of uncertainty is. There are a multitude of possible uses for remotely sensed data that in many cases require applying some parameters that could result in compounding uncertainties (Roy, 2014).

## The Difference between Landsat and MODIS for Users

Landsat data provides temporal depth and spatial detail, which is not available in other biophysical remote sensing products, such as Moderate Resolution Spectral Radiometer (MODIS). However, uncertainty and error estimation are the onus of the end user in the case of Landsat, whereas MODIS provides the end user error estimates as well as quality correction tools. There are two primary sources of uncertainty in the land

surface temperature and other data products generated from Landsat; uncertainty associated with coefficients assigned to bands of Landsat data in generating the land surface temperature layer and uncertainty in the raw digital remote sensing values.

## Sources of Uncertainty in Biophysical Data Derivatives

Land surface temperature derived from Landsat TM, ETM+, and TIRS is the data derivative of focus for this uncertainty analysis. Remote sensing data derivatives which are unscrupulously incorporated into landscape ecological analyses are most likely exposed to propagating errors, resulting in an unknown amount of uncertainty. Quantifying sources of uncertainty is often an overlooked important part of environmental modeling; it has the potential to provide deeper understanding about data, natural phenomena or simulation methods and behavior.

## Motivation for Quantifying Uncertainty in Land Surface Temperature (Ch. 3)

To accurately studying ecosystems and ecosystem change via Landsat remote sensing, one most identify and account for, as much as possible, sources of uncertainty. Due to differences in process scale and observation scale we often have added uncertainty in remote sensing type studies. In addition, because we are recording wavelengths of data in order to measure an ecological trait which is multifaceted and not necessarily directly transferrable to wavelengths we have additional uncertainties to consider.

References

1. Asner, Gregory P., Jonathan MO Scurlock, and Jeffrey A Hicke. "Global synthesis of leaf area index observations: implications for ecological and remote sensing studies." Global Ecology and Biogeography 12.3 (2003): 191-205.

2. Chapin, F. S., Sturm, M., Serreze, M. C., McFadden, J. P., Key, J. R., Lloyd, A. H., ... & Welker, J. M. (2005). Role of land-surface changes in Arctic summer warming. *science*, *310*(5748), 657-660.

3. Ferguson, C. R., Sheffield, J., Wood, E. F., & Gao, H. (2010). Quantifying uncertainty in a remote sensing-based estimate of evapotranspiration over continental USA. *International Journal of Remote Sensing*, *31*(14), 3821-3865.

4. Fisher, Jeremy Isaac, John F. Mustard, and Matthew A. Vadeboncoeur. "Green leaf phenology at Landsat resolution: Scaling from the field to the satellite."Remote sensing of environment 100.2 (2006): 265-279.

5. Forbes, Bruce C., MARC FAURIA, and Pentti Zetterberg. "Russian Arctic arming and 'greening'are closely tracked by tundra shrub willows." Global Change Biology 16.5 (2010): 1542-1554.

6. Hu, Zhenglin, Shafiqul Islam, and Yizong Cheng. "Statistical characterization of remotely sensed soil moisture images." Remote Sensing of Environment 61.2 (1997): 310-318.

7. Huang, C., Goward, S. N., Masek, J. G., Gao, F., Vermote, E. F., Thomas, N., ... & Townshend, J. R. (2009). Development of time series stacks of Landsat images for reconstructing forest disturbance history. *International Journal of Digital Earth*, *2*(3), 195-218.

8. Hyyppä, J., Hyyppä, H., Inkinen, M., Engdahl, M., Linko, S., & Zhu, Y. H. (2000). Accuracy comparison of various remote sensing data sources in the retrieval of forest stand attributes. Forest Ecology and Management, 128(1), 109-120.

9. Lillesand, T. M., Kiefer, R. W., & Chipman, J. W. (2004). Remote sensing and image interpretation (No. Ed. 5). John Wiley & Sons Ltd.

10. Long, J. (2014). *Assessing changes in spatial and temporal patterns of cropping sequences in northeast Montana*. Bozeman, Montana: Montana State University.

11. Markham, B. L., Storey, J. C., Williams, D. L., & Irons, J. R. (2004). Landsat sensor performance: history and current status. Geoscience and Remote Sensing, IEEE Transactions on, 42(12), 2691-2694.

12. Meentemeyer, V., & Box, E. O. (1987). Scale effects in landscape studies. InLandscape heterogeneity and disturbance (pp. 15-34). Springer New York.

13. Moritz, Richard E., Cecilia M. Bitz, and Eric J. Steig. "Dynamics of recent climate change in the Arctic." Science 297.5586 (2002): 1497-1502.

14. Ripley, Brian D. "Spectral analysis and the analysis of pattern in plant communities." The Journal of Ecology (1978): 965-981.

15. Roy, D. P., et al. "Landsat-8: Science and product vision for terrestrial global change research." Remote Sensing of Environment 145 (2014): 154-172.

16. Stumpf, R. P., & Pennock, J. R. (1989). Calibration of a general optical equation for remote sensing of suspended sediments in a moderately turbid estuary.Journal of Geophysical Research: Oceans (1978–2012), 94(C10), 14363-14371.

17. Turner D. P., Ritts W. D., Cohen W. B., Maeirsperger T. K., Gower S. T., Kirschbaum A. A., Running S. W., Zhao M. S., Wofsy S. C., Dunn A. L., Law B. E., Campbell J. L., Oechel W. C., Kwon H. J., Meyers T. P., Small E. E., Kurc S. A. and J. A. Gamon (2005), Site-level evaluation of satellite-based global terrestrial gross primary production and net primary production monitoring, Global Change Biology, 11(4): 666-684

# CHAPTER TWO

## CHANGE DETECTION IN THE DISCONTINUOUS PERMAFROST ZONE USING LANDSAT: HAVE SURFACE FEATURES PRONE TO PRONOUNCED METHANE EFFLUX INCREASED IN SPATIAL EXTENT?

### Contribution of Authors and Co-Authors

Manuscript in Chapter Two

Author: Aiden Johnson

Contributions: Manuscript writing, editing, and formatting.

Co-Author: Dr. Paul Stoy

Contributions: Manuscript edits, data analyses advice, figure improvement suggestions.

Co-Author: Dr. Nathaniel Brunsell

Contributions: Data analysis instruction, helpful comments on clarity of analyses interpretation and methods.

Co-Author: Dr. Stephanie Ewing

Contributions: Manuscript edits, results interpretation guidance, conceptual development instruction of analysis.

Manuscript Information Page

Aiden Johnson, Paul Stoy**,** Nathaniel Brunsell, Stephanie Ewing, Scott Powell, and Mark Greenwood
Remote Sensing
Status of Manuscript:
__x__ Prepared for submission to a peer-reviewed journal
____ Officially submitted to a peer-review journal
____ Accepted by a peer-reviewed journal
____ Published in a peer-reviewed journal

Published by Multidisciplinary Digital Publishing Institute

# CHANGE DETECTION IN THE DISCONTINUOUS PERMAFROST ZONE USING LANDSAT: HAVE SURFACE FEATURES PRONE TO PRONOUNCED METHANE EFFLUX INCREASED IN SPATIAL EXTENT?

The following work is currently in progress to be submitted for publication

Aiden Johnson [1], Paul Stoy [1], Nathaniel Brunsell [2] , and Stephanie Ewing [1]

[1] *Dept. of Land Resources & Environmental Sciences, Montana State University, 325 Leon Johnson Hall, Bozeman MT 59717, USA*

[2] *Dept. of Geography, University of Kansas, 1475 Jayhawk Blvd., 214B Lindley Hall*

## Abstract

Initial airborne methane measurements from the NASA CARVE (Carbon in Arctic Reservoirs Vulnerability Experiment) project have identified lowland peatlands in the Innoko National Wildlife Refuge in west-central AK as having the highest magnitude of methane efflux of any area measured to date (Miller, Dinardo, & Science Team, 2013). The Innoko region is in the discontinuous permafrost zone and is characterized by pronounced permafrost thaw and methane release over decadal to century timescales (Johnston, Ewing, Harden, Varner, Wickland, Koch, & Jorgenson, 2014). Intermediate-aged bog features have been found to produce methane efflux from two to three orders of magnitude higher than that of other bog features. (Johnston et al, 2014). This research, asks: can we classify the landscape based on geomorphic age classes, in order to detect change through time, identifying shifts from frozen forested plateaus to intermediate-aged bogs? Additionally, can we detect landscape feature changes outside of a standard geomorphic pixel based classification method? We classified the landscape using a

Random Forest classification tree for an early date Landsat satellite scene as well as a later date Landsat satellite scene. The results of this classification were dominated by hydrologic features, with a 0.05 increase in mean albedo, essentially no change in both mean Normalized Difference Vegetation Index (NDVI) and mean Brightness Temperature (BT). These results did not definitively answer our question about thermal expansion of bog features over the time period analyzed. Wavelets analysis was applied to the image date differences for albedo, NDVI, and BT in an attempt to quantify the spatial scales of variance. The scale of variance as illustrated by the wavelets analysis for NDVI shows mostly even variance across spatial scales with greatest amount of variance around 4.5 to 5 km. Brightness Temperature had three peaks of high variance between 0.06km - 1 km including maximum variance at about 0.5 km and a pair of peaks between 3 and 4 km. These results brought to light the differing scales of variance depending on the variable being considered, despite the data being collected in the same way.

**Keywords:** change detection; radiometric surface temperature; remote sensing; spectral reflectance; wavelet decomposition

## Introduction

Warming-induced changes to vegetation composition, surface energy exchange, carbon dioxide flux, and methane flux and other factors have the potential to positively feed back to further surface and atmospheric warming in high latitude ecosystems (Chapin et al. 2005, McGuire, Anderson, Christensen, Dallimore, Guo, Hayes, & Roulet,

2009; Schurr, Vogel, Crummer, Lee, Sickman, & Osterkamp 2009). Many of these changes interact with permafrost thaw in poorly understood ways, have occurred since the advent of the satellite record, and are visible on the surface (Jorgenson & Osterkamp 2004). Detecting permafrost thaw itself from space remains challenging, but surface feature changes consistent with permafrost thaw can be quantified for an improved understanding of recent changes to high latitude regions, and consequences of these changes to ecological and Earth system processes.

Understanding changes to the surface-atmosphere exchange of methane is of particular importance because of its large greenhouse warming potential (GWP). Observed circumpolar increases in temperature have resulted in widespread methane release, especially in high-latitude peatlands dominated by permafrost thaw (Christensen, Ekberg, Strom, Mastepanov, Pnaikov, Oquist, & Oskarsson 2003), but quantifying changes to methane flux remains challenging because of the complex biological, chemical, and physical controls over its release. (Christensen, et al 2003; Anthony, Zimov, Grosse, Jones, Anthony, Chapin III, & Frolking, 2014; Mastepanov, Sigsgaard, Dlugokencky, Houweling, Ström, Tamstorf, & Christensen, 2008).

Initial airborne methane measurements from the NASA CARVE (Carbon in Arctic Reservoirs Vulnerability Experiment) project have identified lowland peatlands in the Innoko National Wildlife Refuge in west-central AK as having the highest magnitude of methane efflux of any area measured to date (Miller et al., 2013). The Innoko region is in the discontinuous permafrost zone and is characterized by pronounced permafrost thaw and methane release over decadal to century timescales (Johnston et al., 2014). These

differences are driven by the interaction of hydrology with geologic substrate in geomorphic types with and without permafrost. Vegetation change associated with permafrost thaw can be examined through sequences of "age since thaw" collapse-scar bogs. Intermediate-aged (~20-100 y since thaw) bog features have been found to produce methane efflux from two to three orders of magnitude higher than that of other bog features (Johnston et al., 2014). This research asks if we can classify the landscape based on geomorphic age classes and detect change through time. The challenge from the remote sensing standpoint for determining changes to intermediate bogs is their characteristically small spatial extent – on the order of 50-250$m^2$ (Johnston et al., 2013). Identifying the extent of and transitions to intermediate-aged bogs is critical for understanding the mechanisms underlying geomorphic transitions as well as for interpreting the potential for regional and global climate feedbacks.

## Methods

We first describe the study site and field-sampling campaign followed by an explanation of the remotely sensed data and derived data products. We then describe the change detection analysis methods including a Random Forests supervised classification and pattern change detection using discrete wavelet analysis.

The Innoko Flats National Wildlife Refuge (hereafter 'Innoko') is located within the discontinuous permafrost zone in interior Alaska (Figure 2.1). This study is focused on a 330 $km^2$ area centered at 65.5734° N, -157.72558° W a location where surface reflectance measurements have been made (Johnston et al., 2014; Stoy et al., 2012).

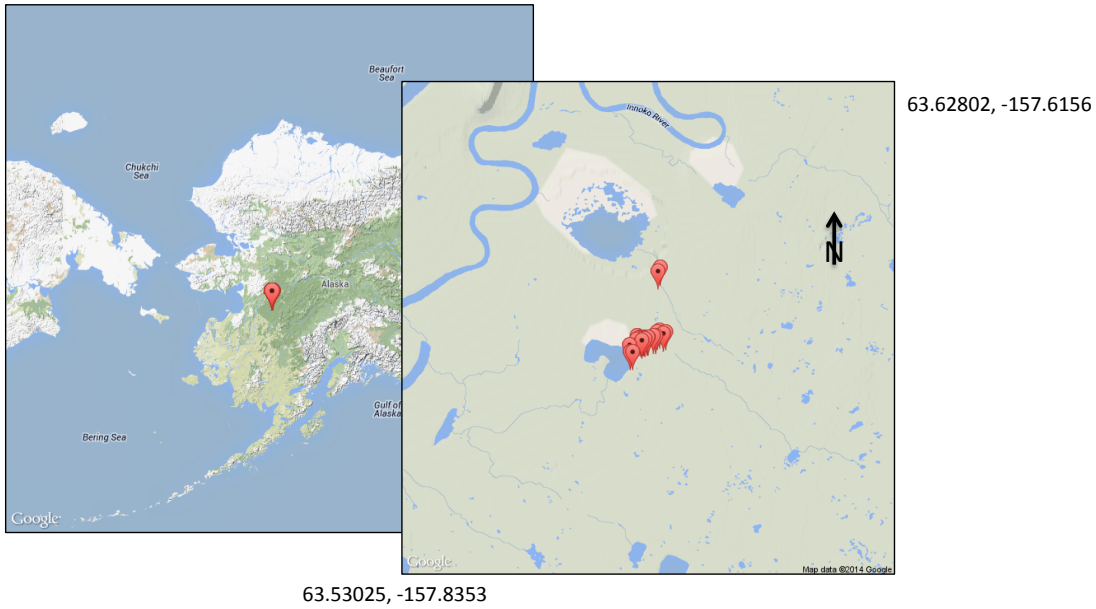


Figure 2.1. Study site location. (a) Overview of Alaska, USA(Google Maps 2013); (b) Map of study site location and ground sample points in the Innoko Flats National Wildlife Refuge (Google Maps 2013).

The ecosystem types present include black spruce dominated forests and lowland birch forests, both of which are associated with the presence of permafrost, as well as collapse scar fens, and progression stage dated bogs. A discernible over-story is present in the frozen features, but not in the bog and fen features. The over-story is dominated by black spruce (*Picea mariana*) with minimal occurrence of white spruce (*P. glauca*) and tamarack (*Larix laricina*). The understory species include Labrador tea (*Rhododendron subarcticum*), bog blueberry (*Vaccinium uliginosum)*, lignonberry (*V. vitis-idaea*), feathermoss (*Hylocomium splendens*), reindeer lichen (*Cladonia arbuscula*) and several *Sphagnum* spp. mosses.

Bog features can be characterized by time since permafrost thaw as described by Johnston et al. 2014, who used radiocarbon and 210Pb to estimate ages of feature types

(up to three replicates per type). That work found that young bogs had formed some 10-20 years ago and were small – on the order of 2.0 $m^2$ - depressions within the permafrost plateau dominated by *S. riparium*, and *S. lindbergii*. Intermediate bogs are larger, on the order of 250 $m^2$, formed some 20-100 years ago, and are dominated by the aerenchymatous *Eriophorum scheuchzeri,* as well as *S. riparium,* and *S. lindbergii*. Old bogs are larger, some 500 $m^2$ on average, with hummocky microtopography and vegetation *Andromeda polifolia, Oxycoccus microcarpus, Carex rotundata, S. balticum,* and *S. flexuosum*. The lowland fen features reflect slow-moving hydrologic flow networks with vegetation dominated by *Carex limosa, C. rotundata, Eriophorum scheuchzeri, S. papillosum,* and *S. majus*.

We de-emphasize the study of young bog formation as the extremely small size of these features and position in the understory of the frozen forest plateaus make change detection from Landsat satellite data unlikely. Instead, we seek to quantify the formation of intermediate bogs given their extreme importance to methane efflux.

## Sampling

Ground observations of the forest plateau understory, young bogs, intermediate bogs, and old bogs were made during a field campaign in September 2010. The sample sites were located as part of the study reported by Johnston et al. (2014), focused on characterizing the thaw characteristics of thermal karst bogs and an adjacent fen. The geographic locations of the geomorphic features were recorded using a field grade geographic positioning system (GeoXR, Trimble). Three replicates of each geomorphic

type were identified for a total of 15 sites. Surface albedo, incoming and outgoing long-wave and shortwave radiation were measured over a period of eight days using a four-component radiometer (Hukseflux). The entire field sample area is less than 5 $km^2$ with lake bordering the west edge and the fen bordering the east side.

The sample locations and their associated ecosystem feature types were used to extract data from remotely sensed data products. These extracted samples from the remotely sensed derived products provided training samples for the random forests supervised classification of the remote sensing data. Based on the unique vegetative characteristics of the geomorphic feature types and their associated thermal properties; we use satellite data to inform our classification of the landscape. The Normalized difference vegetation index (NDVI) is useful to compare greenness and brownness properties, and the brightness temperature (BT) and albedo informs our understanding of surface thermal balance properties.

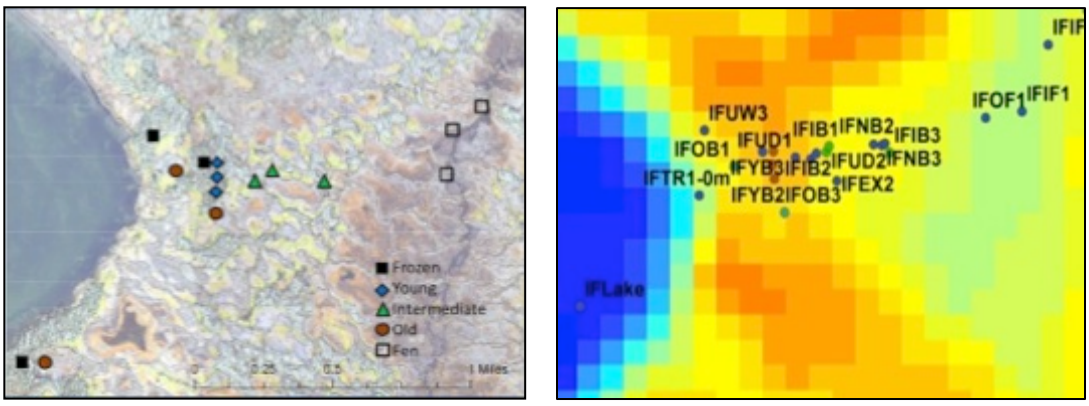


Figure 2.2. (a) Innoko high-resolution aerial photo with ground observations overlain, (figure is from Johnston et al. 2014). (b) Innoko Landsat 5 TM brightness temperature with ground observations overlain.

## Remote Sensing Data

Landsat data were downloaded from the USGS GLOVIS website. The Landsat return interval is 16 days, which enables five to six scenes per snow-free season to be obtained for each year. However clouds limited data usability to one scene for the first 10 years and five scenes in the years from 2000-2011. Data acquisition was limited because the snow free period went from July to the first week of September. For this analysis we classify surface features and interpret changes in spatial patterning for the earliest possible cloud-free scene from June 15, 1985, and the latest possible cloud-free scene with comparable phenologic timing is from July 3, 2009. This provides a 24-year window with which to analyze changes in the spatial extent and patterning of surface features in the Innoko region.

Brightness temperature (BT) is the top of atmosphere temperature and was derived from the thermal spectral band (10.40-12.50 μm) using both Landsat 5 TM and ETM+ data following the approach of Chander et al. (2009):

$$BT = K_2 \ln(K_1 L\lambda)+1 \qquad (1)$$

where $K_1$ and $K_2$ are calibration constants [607.76W/(m$^2$ sr μm)], [1260.56W/(m$^2$ sr μm)] respectively and Lλ is spectral radiance at the sensor's aperture. The calibration constants for ETM+ k1 and K2 are [666.09W/(m$^2$ sr μm)], [1282.71W/(m$^2$ sr μm)] respectively.

Normalized difference vegetation index (NDVI) is an indication of vegetative greenness generated from a fraction of the red spectral band and near infrared spectral band.

$$NDVI = \frac{NIR-RED}{NIR+RED} \qquad (2)$$

where NIR is the near-infrared band and RED is the red portion of the electromagnetic spectrum. Green vegetation absorbs highly in the red portion of the EM spectrum and reflects highly in the infrared portion producing values close to one and ranging down to zero for less green vegetation. A shortwave broadband albedo layer was generated from the Landsat scenes following the method developed by (Liang, 2001). Specifically,

$$\alpha_{short} = \frac{0356\rho_1+0.130\rho_3+0.085\rho_4+0.072\rho_5+0.072\rho_7-0.0018}{0.356+0.130+0.373+0.085+0.072} \quad (3)$$

where $\rho_1$ represents Landsat band 1 and 3 represents Landsat band 3 and so on. Notice band 2 (green) and band 6 (thermal band) are not included. Albedo is a measure of the reflectivity of a surface, a blackbody object which is a perfect absorber has an albedo of zero, an object which is a perfect reflector of incoming radiation it has an albedo of one. Albedos on the Earth surface range from 0.03 for clear water to 0.95 for fresh snow (Bonan, 2002). Darker surfaces tend to have lower albedos like coniferous forests whereas, brighter surfaces like deserts tend to have higher albedos. The amount of incoming solar radiation that is absorbed is what is available for sensible and latent heat flux.

## Change Detection Methods

### Random Forests Classification

A supervised classification of the Landsat data was implemented in order to attempt to distinguish the geomorphic features within each date of imagery. Using the sample data collected in the field campaign, three samples of each surface feature type were used to extract training samples for the Landsat-derived BT, NDVI, and albedo.

These training samples provided a total of 15 input cells into the random forests classification algorithm (Breiman, 2001). The 'randomForest' package in R (*www.r-project.com*) was used for applying the classification and all data were manipulated using the 'maptools' (Bivand and Lewin-Koh, 2014), 'Sp' (Pebesma and Bivand, 2005), and 'raster' (Hijmans, 2014) packages.

Random Forests involves a suite of classification trees that requires the user to define the classes a priori which is a supervised classification method. Bagged classification trees separate the data in q-dimensional space based on the set of samples provided in the training data. The predictor data are the extracted values of NDVI, BT, and albedo and the response is geomorphic feature class. Each feature type made up a class, the classes were grouped as follows: fen, frozen forest/young bog, old bog, and intermediate bog. The random forests classification built using the training data is applied to remaining pixels in the landscape based on the specific pixel location values of NDVI, BT and albedo. The result is an entire image classified as: fen, frozen forest/young bog, old bog and intermediate bog.

The classification was applied to both the 1985 and the 2009 Landsat data. The samples used to train the classifier in each case were extracted from the same date imagery. The spatial area classified into each class was then compared between 1985 and 2009. The result of this comparison led to the next research question, specifically; can we detect landscape feature changes outside of a standard geomorphic pixel based classification? If we are able to isolate the spatial scales of variability and correlate those

to scales of geomorphic feature types, then change detection over the 24 year period may be possible outside of a supervised classification.

Pattern Change Analysis:
A Wavelet-Based Approach

Wavelets analysis is a multi-resolution method for investigating spatial or temporal data. The wavelet provides transposed view of the signal at increasing levels of detail. The signal in this case is the Landsat remote sensing data across the image horizontally, vertically, and then diagonally. This type of analysis is better suited for the non-linear patterning of the landscape than a pixel based approach. Wavelet transform allows analysis of a data series that contains non-stationary power at several different frequencies (Daubechies, 1992). Wavelets analysis is an application of applying a filter to the data at iteratively hierarchical scales. Each level of filtering generates a subsequent set of coefficients representing the data as detail coefficients and approximation coefficients at each scale. This analysis used the Daubechies discrete 2-dimension wavelet transform given by equations 4 & 5. A wavelet is a function of t (usually time, but spatial location in this case) with zero average, which is dilated with a scale parameter s, and translated by u (Mallat, 1999).

$$\psi_{u,s} = \frac{1}{\sqrt{s}} \left(\frac{t-u}{s}\right) \tag{4}$$

The wavelet transform of a function f at the scale s and time or spatial position u is then computed by correlating f with a wavelet.

$$W_f(u,s) = \int_{-\infty}^{+\infty} f\,(t)\, \frac{1}{\sqrt{s}} \psi^* \left(\frac{t-u}{s}\right) \tag{5}$$

Equation 5 is the continuous wavelet transform, as a transform can be calculated for every possible real value of s and u. In this project, we have implemented a Daubechies wavelet family. In the algorithm, a discrete signal is decomposed in a lower scale approximation A and detail scale coefficients as D. This is done by performing a discrete convolution of a low (h) and a high pass filter (g) with the original signal, combined with a binary subsampling. Both low- pass and high-pass filters can be derived from the mother wavelet (Daubechies, 1992). The decomposition formula with $A_o$ the original signal and i a discrete position index iterating over all values in the image, are given in equations 6 and 7 below.

$$A_{i\,[k]} = \sum_{i=-\infty}^{+\infty} h[i-2k]\, A_o[i] \tag{6}$$

$$D_{i\,[k]} = \sum_{i=-\infty}^{+\infty} g[i-2k]\, D_o[i] \tag{7}$$

By iteratively applying equation 6 and 7 to consecutive approximations, starting with $A_o$, the original signal, the signal is decomposed in approximation and detail coefficients at scale levels 2, 4, 8, 16, and so on. The one-dimensional decomposition is easily extended to the two-dimensional case. First, formulas 4 and 5 are applied to an image in the horizontal direction, yielding a set of approximation and detail coefficients for the rows. By applying the same equations to the columns of these first approximations and details, four new images are obtained, a single approximation image and a horizontal, vertical, and diagonal detail images. Due to their superior space-scale localization and their ability to characterize stationary and non-stationary signals, wavelets are an improved method for estimating spatial heterogeneity across multiple scales (Akansu & Haddad, 2000).

## Results and Discussion

### Random Forests Classification

The classification version of the random forests algorithm was implemented in a supervised classification of the remote sensing data. The classification consisted of four geomorphic classes: fen, frozen, intermediate aged bog, and old bog. These geomorphic classes are estimates of time since previously frozen. As the bogs thaw they expand laterally and vertically in extent leading to differing biota on the surface. It has been observed by others (Gislason, Benediktsson, & Sveinsson, 2006) that the Random Forests classification method performs best in dichotomous situations with two classes. Review of the output of the early image classification revealed a three-class result where as the later date classification resulted in a two-class result. The classifier performed reasonably well, classifying the fen and hydrologic features in one class in both the early and late scenes. The early date classification in Figure 2.3 (a) and (c) grouped the pixels into the fen, frozen forest/young bog, and intermediate-aged bog classes. This is in contrast with the late date image classification displayed in Figure 2.3 (b) and (d), in which the only two classes present were fen and intermediate-aged bog. The change in the landscape as indicated by change between these two date classifications is a transition from frozen forest/young bog aged feature class to intermediate-aged bog class. The areal extent for those pixels in the fen class (which is predominately standing water) does not change from 1985-2009. This result indicates that the areal extent of the hydrologic features is consistent providing support for the dates chosen for this change detection as phenologically similar. Those pixels that were in the frozen forest/ young bog class in the

early scene transitioned to the intermediate-aged bog class in the later scene. The sum of spatial area that has transitioned from the frozen forest/young bog to intermediated-aged bog is 90 km. The spatial extent of this transition could be much larger considering the spatial patterning of these landscapes. The classification appears to be broken into two classes, land and water. From here forward we have removed the water pixels from the Landsat derived NDVI, BT, and albedo and are comparing the differences of those pixels across the temporal scale.

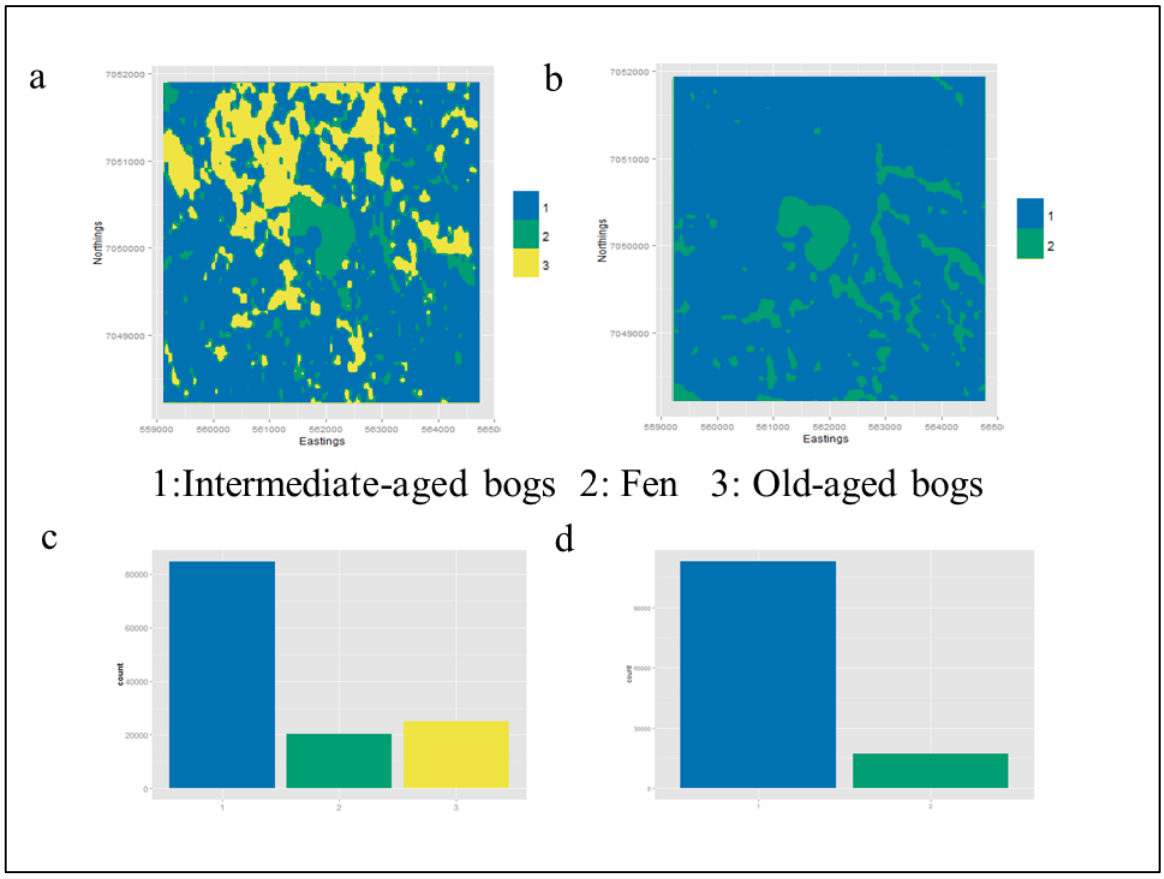


Figure 2.3. (a) Random Forests Classification Results for 1985, where each of the four whole numbers is one class. Number 1 is intermediate-aged bogs, 2 is fen, and 3 is old bogs. (b) Random Forests Classification Results for 2009, the same classification numbers apply for the feature classes (c) The pixel count for 1985 classification results. (d) The pixel counts for classification results of the 2009 imagery.

## Albedo Analysis

The results of the supervised classification raise the question of whether the albedo difference analysis will follow suit in indicating greater numbers of higher albedo values associated with intermediate-aged bogs in the later date albedo image. In fact, we see exactly that response: The pixels that were grouped in the frozen category in the classification have higher albedo values than those in the fen or intermediate classes in the early image classification. In Figure 2.5 we can see the probability of each pixel for both dates of imagery having some albedo values within the range of albedos present in the imagery. There are more albedo values in the higher range the 2009 image than the 1985. This suggests a transition in the non-water portions of the landscape transitioning from lower albedo thus less reflective surfaces to higher albedo and more reflective surfaces in terms of incoming shortwave radiation. Figure 2.4 panel C shows the difference in the two dates albedo by pixel coloration, those pixels with warmer colors are areas of greater increase in albedo than those areas of cooler colors which indicate a decrease, changes are statistically non-existent apparently due to random variation alone.

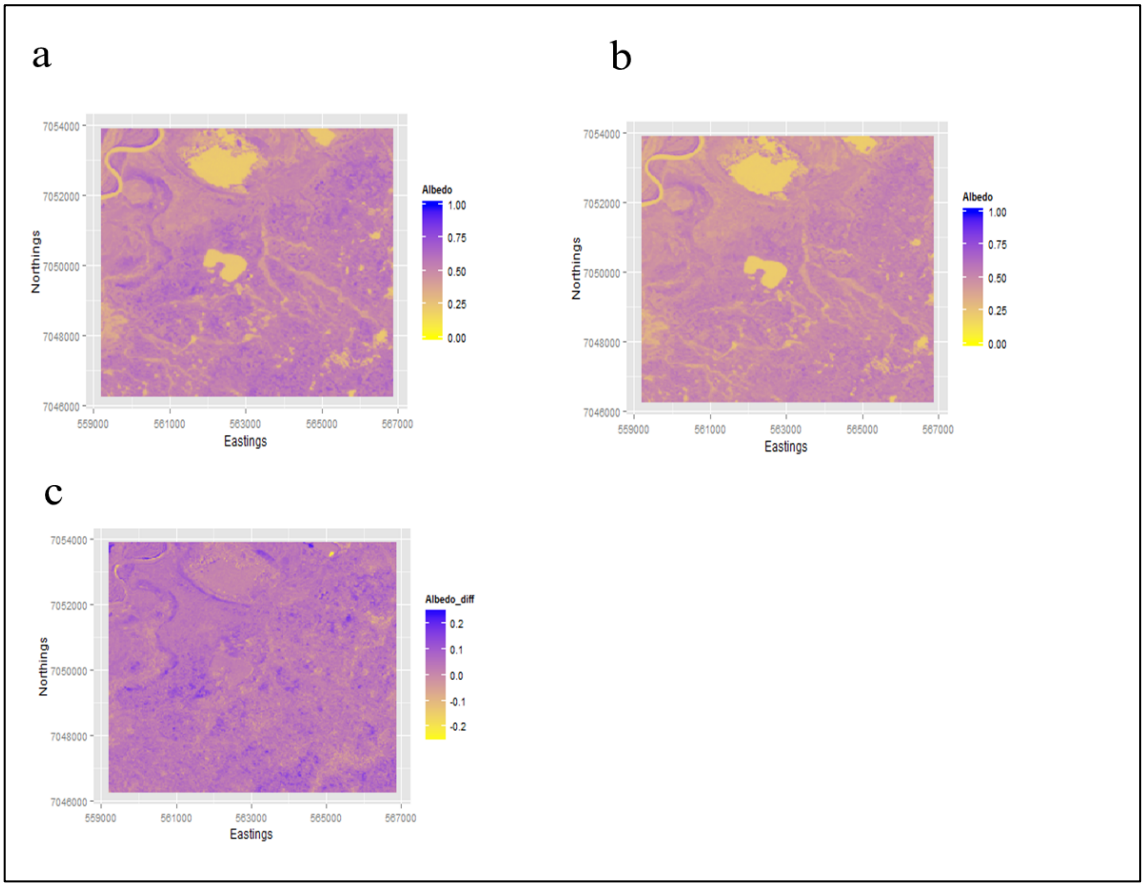


Figure 2.4. Comparison of albedo values for the 1985 and 2009 Landsat images.

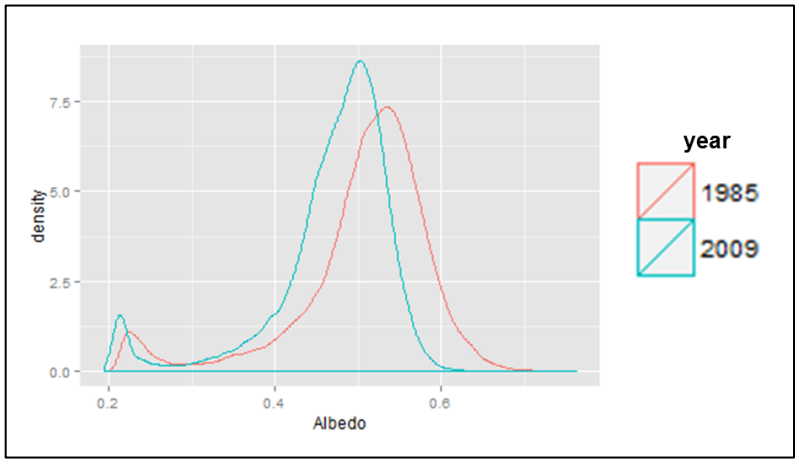


Figure 2.5 Probability distribution functions for both dates of albedo data, excluding water pixels.

## NDVI Analysis

Albedo is a function of the surface characteristics of the site and in natural systems we often see a change in albedo as result of a change in the vegetative community (Mitchell, Manabe, Meleshko, & Tokioka, 1990). We would expect the change in NDVI in Figure 2.6 to also indicate a transition in values that ties closely with the albedo change detection. Interestingly what we actually observe here is the same number of pixels in each NDVI value cohort; there are both increases and decreases. The probability associated with each NDVI value from the early image is the same for the late image. The number of pixels that increased is closely related to the number that decreased and those changes were very small. Further analysis reveals the observed changes in NDVI are spurious and a result of the high level of uncertainty present in Landsat TM band 4.

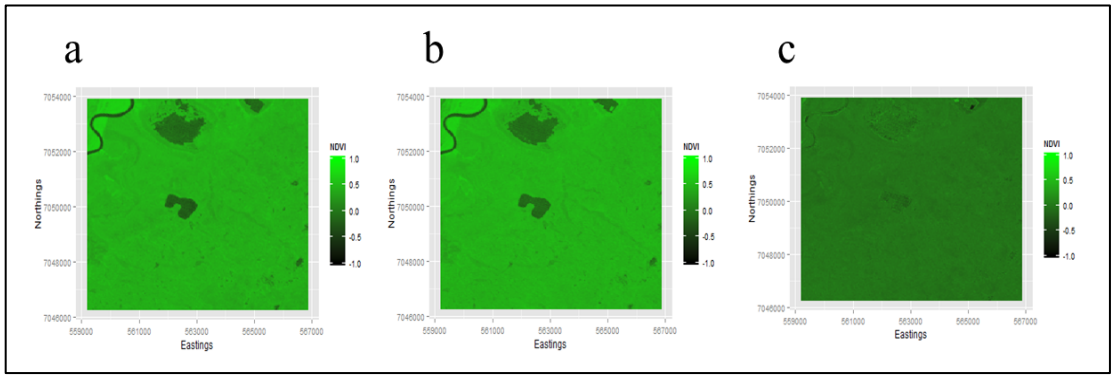


Figure 2.6. (a) Landsat NDVI 1985 (b) Landsat NDVI 2009 (c) Difference between Landsat NDVI 1985 & 2009.

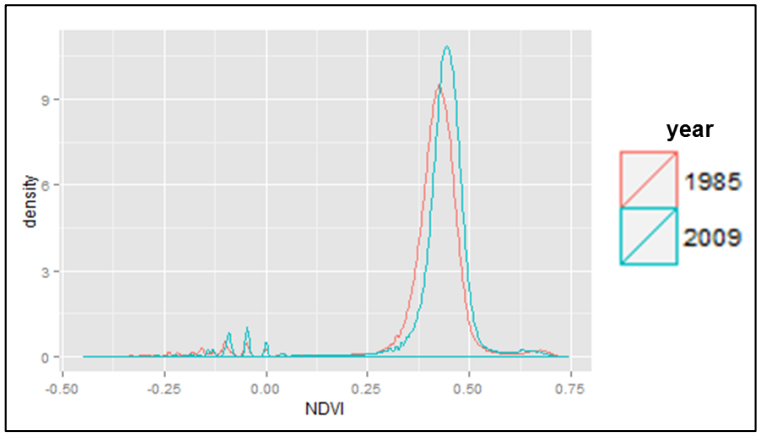


Figure 2.7. Probability distribution functions for NDVI values for 1985 & 2009, excluding the water pixels.

## Wavelet Analysis

The spatial and temporal scales at which plant communities in sub-arctic regions are changing remain uncertain. Here using the wavelet transformation technique we quantify characteristic spatial scales of surface change in order to inform our understanding of spatial scales of change. Regions of increased greenness and increased spatial extent of individual features could indicate areas of active permafrost thaw and establishment of carex spp, sphagnum riparium, and other mosses (Bauer & Vitt, 2011). These vegetative transitions could in turn lead to changes in thermal exchanges. The difference image of BT (Figure 2.8) indicated several larger scaled areas of cooling which suggests the transition in vegetation is having an unexpected affect. This discontinuity between what would be expected, a warming as a result of transitioning from lower albedo species to higher albedo species may be due to a lack of sub-surface conductivity. Species level thermal properties, such as conduction and insulation need to

be considered when evaluating thermal dynamics in a system (Stoy, Street, Johnson, Prieto-Blanco, & Ewing, 2012).

Difference images between 1985 and 2009 for the BT (Figure 2.8) and NDVI (Figure 2.6) were calculated in order to quantify change through time in these variables. These difference images were then analyzed using the discrete wavelets analysis. The red and orange colors in the difference BT image indicates locations of warming, and there are only a few minimal locations of this around a riparian area towards the bottom left of the image. Generally the BT difference image indicates a cooling of ~2°K for the period 1985-2009, however, due to high variability of temperatures we cannot make an inference to a trend of change over time.

The BT level 5 & 6 wavelet coefficients on Figure 2.9 have the greatest range in amplitude and indicate features of interest at a scale of ~ 1km. The smallest scale wavelet coefficient indicate the least amount of variability, the heterogeneity is similar at those scales.

Difference NDVI, Figure 2.6 indicates some minute isolated regions of increased greenness, and a more widespread slight decrease in greenness represented in characteristic patch patterns. NDVI has a consistent variance across spatial scales until above 750m (250 separation distance), increasing and broadening until spiking around 1km (350 separation distance), see Figure 2.10

Compared to the BT wavelet coefficients, the NDVI coefficients in Figure 2.10 are more similar to each other in variability and amplitude ranges with the majority of the variability appears in the 4-6 levels.

As an initial stage in determining spatial scale variability of the difference images, variograms were calculated to elucidate the variability across space in between the two dates of imagery. After examining both the wavelets analysis output and the variability displayed in the variograms most of the variability is captured at the medium to larger spatial extent of about 1 km. The BT variogram indicates a similarity of features at close proximity and an increased variability in features at greater distances (Figure 2.8 (b)).

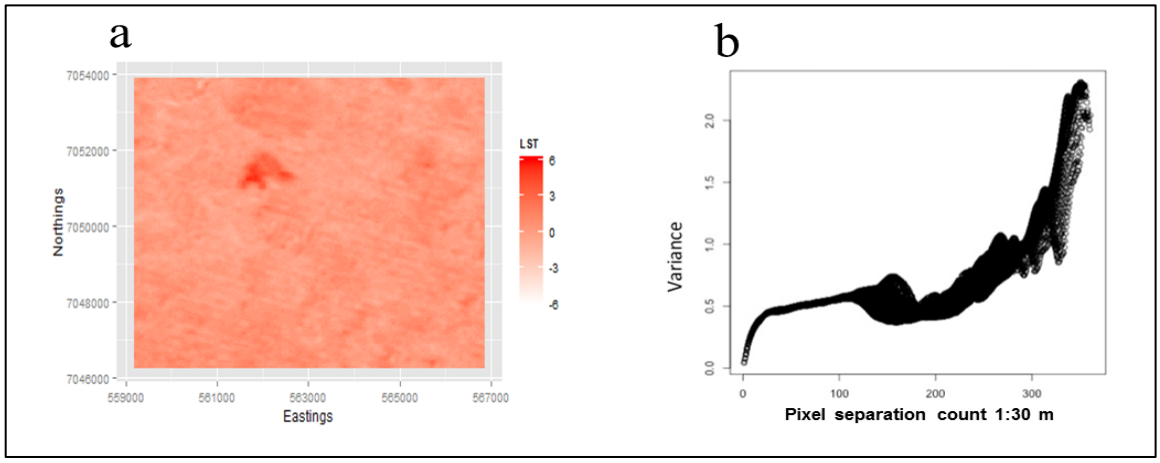


Figure 2.8. (a) Difference of brightness temperature between 1985 & 2009 for subset of Innoko Region displayed previously. (b) Variogram calculated on the 10,000 pixel subset of temperature.

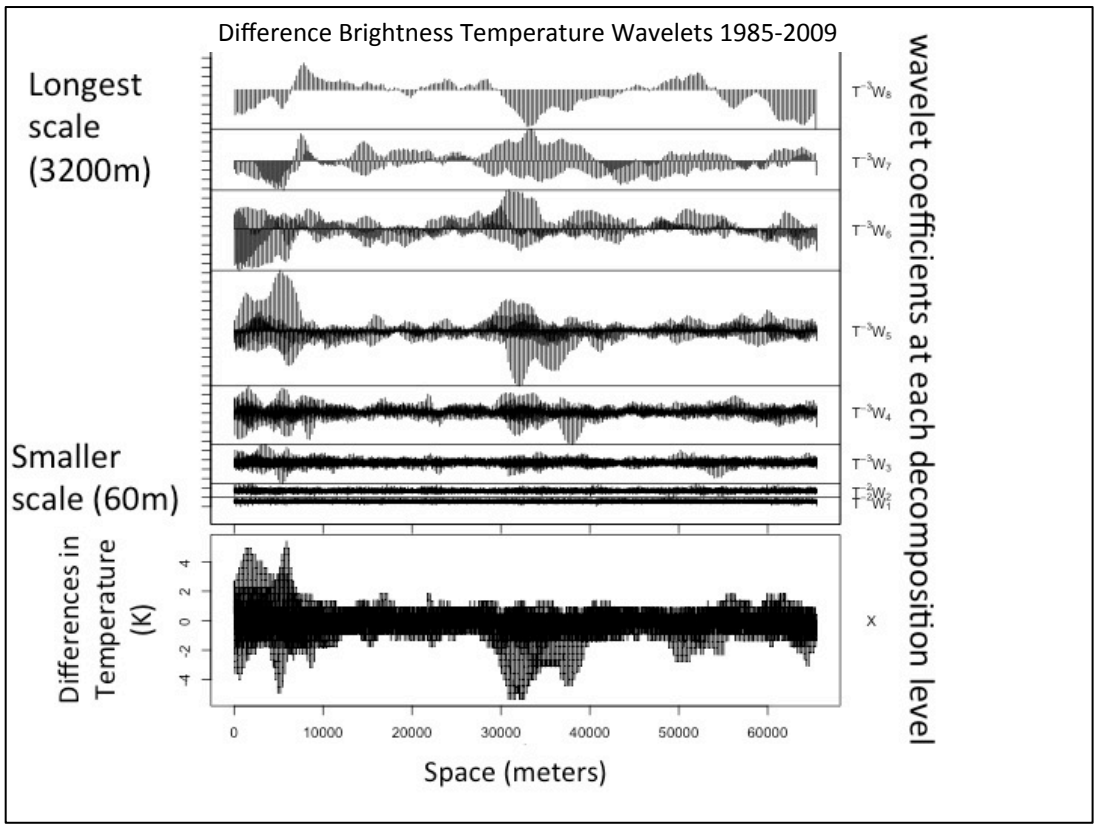


Figure 2.9. Wavelet analysis output from differenced brightness temperatures from 1985 & 2009.

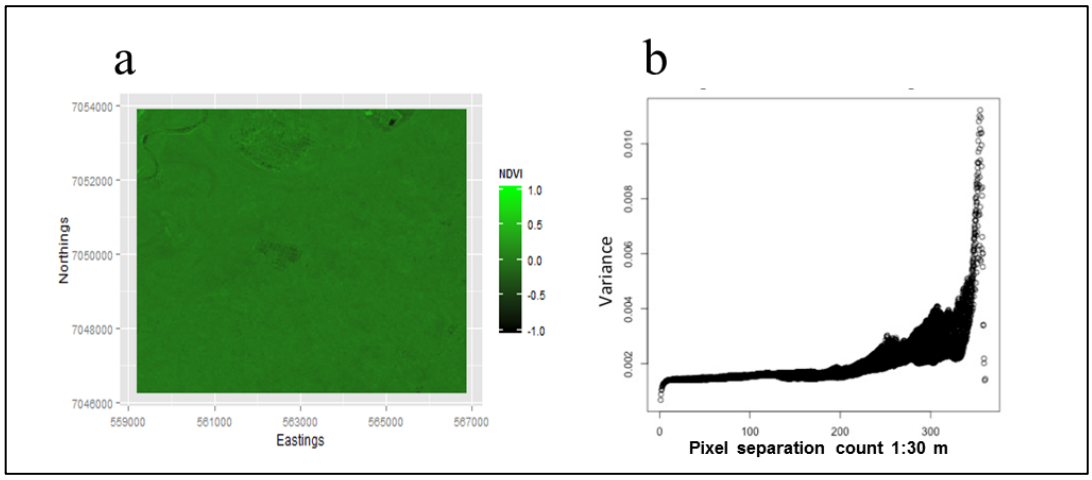


Figure 2.10 (a) Difference of NDVI between 1985 & 2009 for subset of Innoko Region displayed previously. (b) Variogram calculated on the 10,000-pixel subset of NDVI.

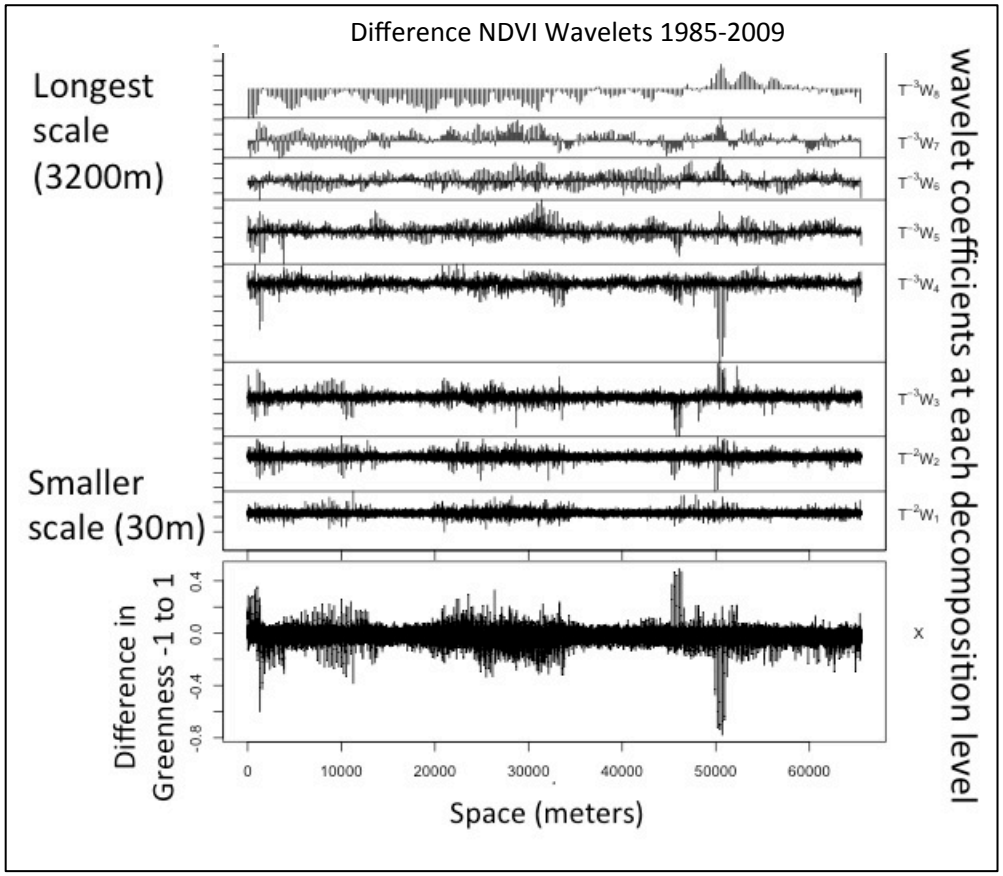


Figure 2.11. Wavelet analysis output from NDVI from 1985 & 2009.

## Conclusions

The results provide little insight into whether there is thermal expansion of bog features into intermediate–aged bogs. There are several reasons for this; firstly the 30 m pixel size of Landsat data has proven to large a level of detail to locate feature specific change. Although, some greater scales of change were found with the wavelets analysis, these scales are difficult to directly tie-back to a feature type classification. Wavelets analysis indicates a spatial scale of variance much greater than that of the geomorphic feature classes pointing to the hydrological features dominating the surface characteristics.

The geomorphic feature classification suffers from the small n problem in this analysis. There are so few samples for training data to inform the Random Forests classifier. More samples within each feature type may have improved the classification to a first order. Hydrologic variability plays a major role in the surface characteristics and must be considered for further remote sensing type analyses.

## Acknowledgments

The Montana Institute on Ecosystems provided financial assistance. PCS acknowledges funding from the National Science Foundation ('Scaling ecosystem function: Novel Approaches from MaxEnt and Multiresolution', Division of Biological Infrastructure #1021095). The state of Montana, U.S. Geological Survey as well as National Science Foundation EAR #0630319 also supported this work.

References

1. Akansu, A.N. & Haddad, P.R., 2000. *Multiresolution signal decomposition:transforms, subbands, and wavelets*, Academic Press.

2. Anthony, K. W., Zimov, S. A., Grosse, G., Jones, M. C., Anthony, P. M., Chapin III, F. S., ... & Frolking, S. (2014). A shift of thermokarst lakes from carbon sources to sinks during the Holocene epoch. *Nature*.

3. Bauer, I.E. & Vitt, D.H., 2011. Peatland dynamics in a complex landscape: Development of a fen-bog complex in the Sporadic Discontinuous Permafrost zone of northern Alberta, Canada. *Boreas*, 40(4), pp.714–726.

4. Bivand, Roger and Lewin-Koh, Nicholas, 2014. maptools: Tools for reading and handling spatial objects. R package version 0.8-30.

5. Bonan, G.B., 2002. *Ecological climatology: concepts and applications*, Cambridge University Press.

6. Breiman, Leo. "Random forests." *Machine learning* 45.1 (2001): 5-32.

7. Chander, G. & Markham, B., 2003. Revised Landsat-5 TM Radiometric Calibration Procedures and Postcalibration Dynamic Ranges. , 41(11), pp.2674–2677.

8. Chander, G., Markham, B.L. & Helder, D.L., 2009. Summary of current radiometric calibration coefficients for Landsat MSS, TM, ETM+, and EO-1 ALI sensors. *Remote Sensing of Environment*, 113(5), pp.893–903. Available at: http://linkinghub.elsevier.com/retrieve/pii/S0034425709000169 [Accessed March 1, 2012].

9. Chapin, F.S. et al., 2005. Role of land-surface changes in arctic summer warming. *Science (New York, N.Y.)*, 310(5748), pp.657–60. Available at: http://www.ncbi.nlm.nih.gov/pubmed/16179434 [Accessed March 17, 2012].

10. Christensen, T. R., Ekberg, A., Ström, L., Mastepanov, M., Panikov, N., Öquist, M., ... & Oskarsson, H. (2003). Factors controlling large scale variations in methane emissions from wetlands. *Geophysical Research Letters*,*30*(7).

11. Christensen, T.R. et al., 2004. Thawing sub-arctic permafrost: Effects on vegetation and methane emissions. *Geophysical Research Letters*, 31, p.L04501.

12. Cutler, D.R. et al., 2012. Random Forests for Classification in Ecology Published by : Ecological Society of America content in a trusted digital archive . We use

information technology and tools to increase productivity and facilitate new forms of scholarship . For more informatio. *Ecology*, 88(11), pp.2783–2792.

13. Daubechies, I., 1992. *Ten lectures on wavelets*, SIAM.

14. Gislason, P.O., Benediktsson, J.A. & Sveinsson, J.R., 2006. Random forests for land cover classification. *Pattern Recognition Letters*, 27(4), pp.294–300.

15. Grosse, G. et al., 2011. Vulnerability of high-latitude soil organic carbon in North America to disturbance. *Journal of Geophysical Research*, 116, pp.1–23. Available at: http://www.agu.org/pubs/crossref/2011/2010JG001507.shtml [Accessed October 28, 2012].

16. Hijams, Robert, 2014. raster: Geographic data analysis and modeling. R package version 2.3-0.

17. Houborg, R., Soegaard, H. & Boegh, E., 2007. Combining vegetation index and model inversion methods for the extraction of key vegetation biophysical parameters using Terra and Aqua MODIS reflectance data. *Remote Sensing of Environment*, 106(1), pp.39–58.

18. Irish, R.R., 2000. Landsat 7 science data users handbook. *National Aeronautics and Space Administration, Report*, pp.415–430.

19. Johnston, C. E., Ewing, S. A., Harden, J. W., Varner, R. K., Wickland, K. P., Koch, J. C., & Jorgenson, M. T. (2014). Effect of permafrost thaw on CO2 and CH4 exchange in a western Alaska peatland chronosequence. *Environmental Research Letters*, *9*(8), 085004

20. Jorgenson, M. T., and T. E. Osterkamp. "Response of boreal ecosystems to varying modes of permafrost degradation." *Canadian Journal of Forest Research* 35.9 (2005): 2100-2111.

21. Kumar, P. & Foufoula-Georgiou, E., 1997. Wavelet Analysis for Geophysical Applications. *Reviews of Geophysics*, 35(4), pp.385–412.

22. Liang, S., 2001. Narrowband to broadband conversions of land surface albedo I Algorithms. *Remote Sensing of Environment*, 76(2000).

23. Liang, S., 2007. Recent developments in estimating land surface biogeophysical variables from optical remote sensing. *Progress in Physical Geography*, 31(5), pp.501–516. Available at: http://ppg.sagepub.com/cgi/doi/10.1177/0309133307084626 [Accessed March 20, 2014].

24. Mallat, S., 1999. *A wavelet tour of signal processing*, Academic press.

25. Malmer, N. et al., 2005. Vegetation, climatic changes and net carbon sequestration in a North-Scandinavian subarctic mire over 30 years. *Global Change Biology*, 11, pp.1895–1909. Available at: http://doi.wiley.com/10.1111/j.1365-2486.2005.01042.x [Accessed August 30, 2012].

26. Mastepanov, M., Sigsgaard, C., Dlugokencky, E. J., Houweling, S., Ström, L., Tamstorf, M. P., & Christensen, T. R. (2008). Large tundra methane burst during onset of freezing. *Nature*, *456*(7222), 628-630.

27. McGuire, A. D., Anderson, L. G., Christensen, T. R., Dallimore, S., Guo, L., Hayes, D.J., ... & Roulet, N. (2009). Sensitivity of the carbon cycle in the Arctic to climate change. *Ecological Monographs*, *79*(4), 523-555.

28. Miller, C.M., Dinardo, S. & Science Team, C., 2013. The Carbon in Arctic Reservoirs Vulnerability Experiment (CARVE): Results from the 2012 Alaska science flights. In *4th North American Carbon Program All Investigators Meeting*.

29. Mitchell, J. F. B., Manabe, S., Meleshko, V., & Tokioka, T. (1990). Equilibrium climate change and its implications for the future. *Climate Change: The IPCC Scientific Assessment*, *131*, 172.

30. Pebesma, E.J. and R.S. Bivand, 2005. sp:Classes and methods for spatial data in R.

31. Schuur, E. A., Vogel, J. G., Crummer, K. G., Lee, H., Sickman, J. O., & Osterkamp, T. E.(2009). The effect of permafrost thaw on old carbon release and net carbon exchange from tundra. *Nature*, *459*(7246), 556-559.

32. Stoy, P. C., Street, L. E., Johnson, A. V., Prieto-Blanco, A., & Ewing, S. A. (2012).Temperature, Heat Flux, and Reflectance of Common Subarctic Mosses and Lichens under Field Conditions: Might Changes to Community Composition Impact Climate-Relevant Surface Fluxes?. *Arctic, Antarctic, and Alpine Research*, *44*(4), 500-508.

33. Torrence, C. & Compo, G.P., 1997. A Practical Guide to Wavelet Analysis. *Bulletin of American Meteorological Society*.

# CHAPTER THREE

## RANDOM UNCERTAINTY IN LAND SURFACE TEMPERATURE CALCULATED USING LANDSAT TM, ETM+, AND TIRS

### Contribution of Authors and Co-Authors

Manuscript in Chapter Three

Author: Aiden Johnson

Contributions: Manuscript writing, editing, and formatting.

Co-Author: Dr. Paul Stoy

Contributions: Manuscript edits, data analyses advice, figure improvement suggestions.

Co-Author: Dr. Lucy Marshall

Contributions: Data analysis instruction, helpful comments on clarity of analyses interpretation and methods.

Co-Author: Dr. Joel McCorkel

Contributions: Conceptual development and instruction of analyses methods.

Manuscript Information Page

Aiden Johnson , Paul Stoy **,** Lucy Marshall, and Joel McCorkel.
Ecological Applications
Status of Manuscript:
__x__ Prepared for submission to a peer-reviewed journal
____ Officially submitted to a peer-review journal
____ Accepted by a peer-reviewed journal
____ Published in a peer-reviewed journal

Published by Ecological Society of America

# RANDOM UNCERTAINTY IN LAND SURFACE TEMPERATURE CALCULATED USING LANDSAT TM, ETM+, AND TIRS.

THE FOLLOWING WORK IS CURRENTLY IN PROGRESS TO BE SUBMITTED FOR PUBLICATION

Aiden Johnson[1], Paul Stoy[1], Lucy Marshall[1,2], Joel McCorkel[3]

[1] *Department of Land Resources and Environmental Sciences, Montana State University, Bozeman, MT 59717*

[2] *School of Civil and Environmental Engineering, University of New South Wales, Australia*

[3] *NASA/GSFC, Greenbelt, MD 20771*

## Abstract

Quantifying random errors in remotely sensed data products is increasingly important as more scientists from diverse disciplines begin to use these data, often with rudimentary knowledge of how these data products are created and their inherent uncertainties. Most work to date has focused on rigorously assessing and correcting bias errors due to sensor drift atmospheric attenuation, surface properties like land surface emissivity, and other sources, all of which are critical for accurate measurements. Random errors remain after minimizing all known bias terms, but have received less attention to date. To quantify random error in a remotely sensed data product, we apply a Monte Carlo routine to the algorithm used to calculate the land surface temperature (LST) product from Landsat 5 (TM), Landsat 7 (ETM+), and Landsat 8 (TIRS). Specifically, we quantify random uncertainty due to sensor accuracy and the MODTRAN

routine used to correct for atmospheric attenuation. A small subset of a Landsat scene within the Judith River watershed in central Montana, USA, was selected for computational efficiency and to avoid the Landsat 7 scan line correction error. The subset represents contains the full range of land cover types present within the watershed including forested upland, crops, and riparian. In order to determine if the Landsat 8 sensor has provided an improved estimate of LST we present two sets of comparisons on days with similar meteorological conditions and prevailing clear skies during the growing season. Day of year 219 (TM) and 211 (TM), 2011, were chosen for the TM/ETM+ comparison, and day of year 184 (ETM+) and 208 (TIRS), 2013 were chosen for the ETM+/TIRS comparison.

For all three Landsat sensors the results indicate the overall uncertainty about the LST product is dominated by random uncertainty and is less a function of the MODTRAN conversion. We find the uncertainty due to the MODTRAN conversion to LST was found to represent between 1.94˚K - 4.42˚K. The results also indicate no substantial difference in uncertainty depending on sensor or with the advent of Landsat 8, surface properties and conditions are deemed a greater source of uncertainty minimizing the effective difference between sensors. Additionally, we have found that as mean temperature increases overall uncertainty increases. This generally linear relationship of about 1% could be applied to approach quantifying the uncertainty about land surface temperature data at a tertiary level.

## Introduction

Remotely-sensed data are subject to bias errors and random errors. Most work to date has focused on rigorously assessing and correcting bias errors due to sensor drift ( Barsi, Barker, & Schott, 2003), atmospheric attenuation (Barsi et al. 2003), surface properties like land surface emissivity, and other sources, all of which are critical for accurate measurements. Random errors remain after minimizing all known bias terms, but have received less attention to date.

Quantifying random errors in remotely sensed data products is increasingly important as more scientists from diverse disciplines begin to use these data, often with rudimentary knowledge of how these data products are created and their inherent uncertainties. Quantifying uncertainty in remotely sensed data products is also important for scientific objectives. Uncertainty estimates are required, for example, to implement data assimilation routines (Hill, Quaife, & Williams, 2011), bridge scales between ground-based and space-based observations (Jarvis, 1995; Stoy, Williams, & Disney, 2009), and detect significant temporal and spatial changes in land surface attributes (Prieto-Blanco, et al. 2009; Kerr & Ostrovsky 2003; Cohen & Goward 2004; Tan, Masek, & Wolfe, 2013). Quantifying random errors, in addition to bias errors, is necessary for a full accounting of uncertainty, and communicating these uncertainties to the ever-growing community of remote sensing data product users is important for appropriate and informed usage of these data.

To quantify random error in a remotely sensed data product, we apply a Monte Carlo routine to the algorithm used to calculate the land surface temperature (LST)

product from Landsat 5 (TM), Landsat 7 (ETM+), and Landsat 8 (TIRS). Specifically, we quantify random uncertainty due to sensor accuracy and the MODTRAN routine used to correct for atmospheric attenuation to address the following questions:

(1) How has the random uncertainty in the LST product changed with advent of new satellites in the Landsat constellation?

(2) Which is a greater source of uncertainty, the satellite observations themselves or the atmospheric corrections used to calculate the LST data product?

(3) Is it possible to create a simple estimate of random uncertainty based on the magnitude of LST?

We focus our analysis on a gradient between agriculturally-dominated landscapes, rangeland, and forest to encompass a wide range of surface types while avoiding the known scan line correction error in Landsat 7 (Coll, 2010).

## Materials and Methods

### Study Site

The study site is in the Judith River watershed in central Montana. The Judith River headwaters are dominated by montane coniferous forests, and dryland cereal and forage production dominate at lower elevations. A small subset within the Judith River watershed was selected for computational efficiency and to avoid the Landsat 7 scan line correction error. The subset represents a transect from forested upland to cropland and riparian areas and was chosen to include the full range of land cover types present within

the watershed. The spatial extent of the study area is 330 $km^2$ and includes an eddy flux tower located at 46.994701 N, 109.613660 W (Figure 3.1).

## Landsat Data

Landsat data were downloaded from the USGS GLOVIS website. Landsat TM and ETM+ data were downloaded for the 2011 growing season for comparison, and Landsat ETM+ and TIRS data were downloaded for the 2013 growing season. As Landsat TM was unavailable after Autumn 2011, and therefore cannot be directly compared to Landsat 8 for which data became available on February, 2013, we present two sets of comparisons on days with similar meteorological conditions and prevailing clear skies during the growing season. Day of year 219 (TM) and 211 (ETM+), 2011, were chosen for the TM/ETM+ comparison, and day of year 184 (ETM+) and 208 (TIRS), 2013 were chosen for the ETM+/TIRS comparison. All three sensors provide multispectral data with 30 m spatial resolutions and are described in detail elsewhere (Irish 2000).

Data from each date was first converted to digital numbers from at sensor brightness then using MODTRAN (Eq.1) and Eq. 2. converted to land surface temperature by applying adjustments for atmospheric attenuation outlined by (Barsi et al. 2003). Uncertainty in the MODTRAN atmospheric adjustment is within 2-3 degrees K (Quattrochi and Luvall 2004). Moderate resolution atmospheric Transmission (MODTRAN) is a computer program originally written in Fortran, used to model atmospheric attenuation and propagation of electromagnetic energy through the

atmosphere, it was developed by the U.S. Air force and is maintained by several US agencies. The equation for calculation is given here:

$$L_{TOA} = \tau\varepsilon L_T + L_u + (1-\varepsilon)L_d \quad (1)$$

where τ is the atmospheric transmission, ε is the emissivity of the surface, LT is the radiance of a blackbody target of kinetic temperature T, Lu is the upwelling or atmospheric path radiance, Ld is the downwelling or sky radiance, and LTOA is the space-reaching or TOA radiance measured by the instrument. Radiances are in units of W/m2ster·μm and the transmission and emissivity are unitless. Landsat radiances were then converted to land surface temperature in Kelvin following Chander, Markham, & Helder (2009):

$$LST=K_2 \ln(K_1 L\lambda) \quad (2)$$

where $K_1$ and $K_2$ are calibration constants that differ among sensors (see Table 3.2) and Lλ is spectral radiance leaving the Earth's surface. $K_1$ and $K_2$ are derived from Planck's Law and contribute little random uncertainty to the final LST product. The LST product can be seen in Figure 3.2 as it is generated following the MODTRAN adjustment and Planck's law conversion to temperature. This is the land surface temperature data typically used in remote sensing studies that require the spatial scale of Landsat (30 m) rather than MODIS or some other larger spatial scaled temperature data.

## Monte Carlo Uncertainty Analysis

There are two primary sources of random uncertainty in Landsat-derived LST: uncertainty in the raw digital remote sensing values and uncertainty in the MODTRAN

estimate of atmospheric attenuation across the thermal bands. To quantify the uncertainty associated with sensor measurements and atmospheric attenuation in Eq. (1), a Monte Carlo method of random parameter generation was applied. The Monte Carlo approach applied here uses a defined distribution, here a Gaussian distribution with variance of 2˚ Kelvin as found by (Quattrochi and Luvall 2004) , and random draws to select multiple realizations of likely parameter sets and the subsequent MODTRAN parameters of Ld, Lu, and Tau. One thousand iterations of the MODTRAN values were created for each pixel of each Landsat scene subset the resulting distributions are shown in Figure 3.3. We assume that the parameter values $K_1$ and $K_2$ contribute trivial amounts of uncertainty – apart from rounding error - as they are calculated directly from Planck's Law.

The next step was to generate LST products for each sensor subset using the distributions of values and finding the means and variances of the stacks of images for each sensor. In, Figure 3. 3 we have the mean LST's in upper four panels and variances in lower four panels. Here we can compare the range of values for each sensor and their associated variance. The temperatures range from 310˚K - 289˚K, well within what would be expected for this region and season. The variances are also quite similar across sensor, excluding the ETM 211, ranging from 2˚K to 4.5˚K, but with most of pixels falling in the less than 4 degrees range. Similarly if we subtract the mean LST images generated from the MC routine from the LST images generated by the specific MODTRAN suggested adjustments we can see in Figure 3.4 there is little difference in the results across sensors, illustrating the effect of added uncertainty from MODTRAN is minimal and the real difference in variance has more to do with the specific image itself.

## Results

Uncertainty due to the MODTRAN conversion to LST was found to represent between 1.94˚K - 4.42˚K, see Table 3.3. For both Landsat TM and ETM+ this result indicates the overall uncertainty about the LST product is dominated by random uncertainty and is less a function of the MODTRAN conversion.

### Uncertainty within Subsets of Landsat Scenes

Maps of calculated LST for both study dates are presented in Figure 3.3 & 3.4. The mean temperatures are similar across both comparisons three sensors, as they are seasonally similar. The maps provide some contextual perspective; we can see the warmer temperatures are found in the croplands and rangeland areas, where as the cooler areas are the riparian and slightly elevated forested areas in blues. There is also a single pivot irrigated field which is also bright blue and subsequently *ca.* 10˚K cooler than the surrounding areas for all images.

The results indicate there is no significant decrease in the uncertainty in transition from TIRS to ETM+. These analyses found a decrease in uncertainty in Landsat ETM+ as compared to its predecessor Landsat TM. Figure 3.3 displays the mean and variance for each Landsat sensors for the subset region. The proportion of uncertainty associated with MODTRAN was fairly consistent increasing slightly when total variance increased in the scene and as temperatures increased as well. Reviewing Figure 3.4 we can see the remaining variability after taking the difference between the date specific MODTRAN calculated LST and the Monte Carlo simulated mean LST.

## Discussion

The improvements in sensor design in Landsat TIRS for thermal band are a significant finding that should be considered for any future land surface temperature analyses. It is clear that Landsat TIRS has improved in terms of uncertainty not associated with the MODTRAN translation; however, it cannot be clearly distinguished as an improvement in the sensor versus a general landscape decrease in variance for the time period reviewed. Future analysis should involve multiple landscapes and climatic regions for transferability analysis of findings.

The non-linear relationship of the MODTRAN correction has resulted in an increase width in the distribution of values for land surface temperature. This method of radiative transfer in order to incorporate atmospheric attenuation adjustment is expected to cause an increase in the land surface temperature uncertainty however this is necessary adjustment to gain a value for temperature at the surface of the Earth.

The data themselves are found to be the greatest source of uncertainty in these analyses. Relying on atmospheric adjustments and Planck's law translations does not substantially impact the resulting land surface data negatively.

Additionally, we have found that as mean temperature increases overall uncertainty increases. This generally linear relationship of about 1% could be applied to approach quantifying the uncertainty about land surface temperature data at a tertiary level.

The level of uncertainty found in these land surface temperature analysis can be extended to other Landsat derived data products. The linear relationships linking spectral

responses to biophysical properties always have an associated uncertainty. Understanding and reporting the variance associated with derived products is necessary for interpretation of actual change versus randomness. The level of estimated uncertainty helps elucidate the reasonable level of inference for a Landsat derived data products.

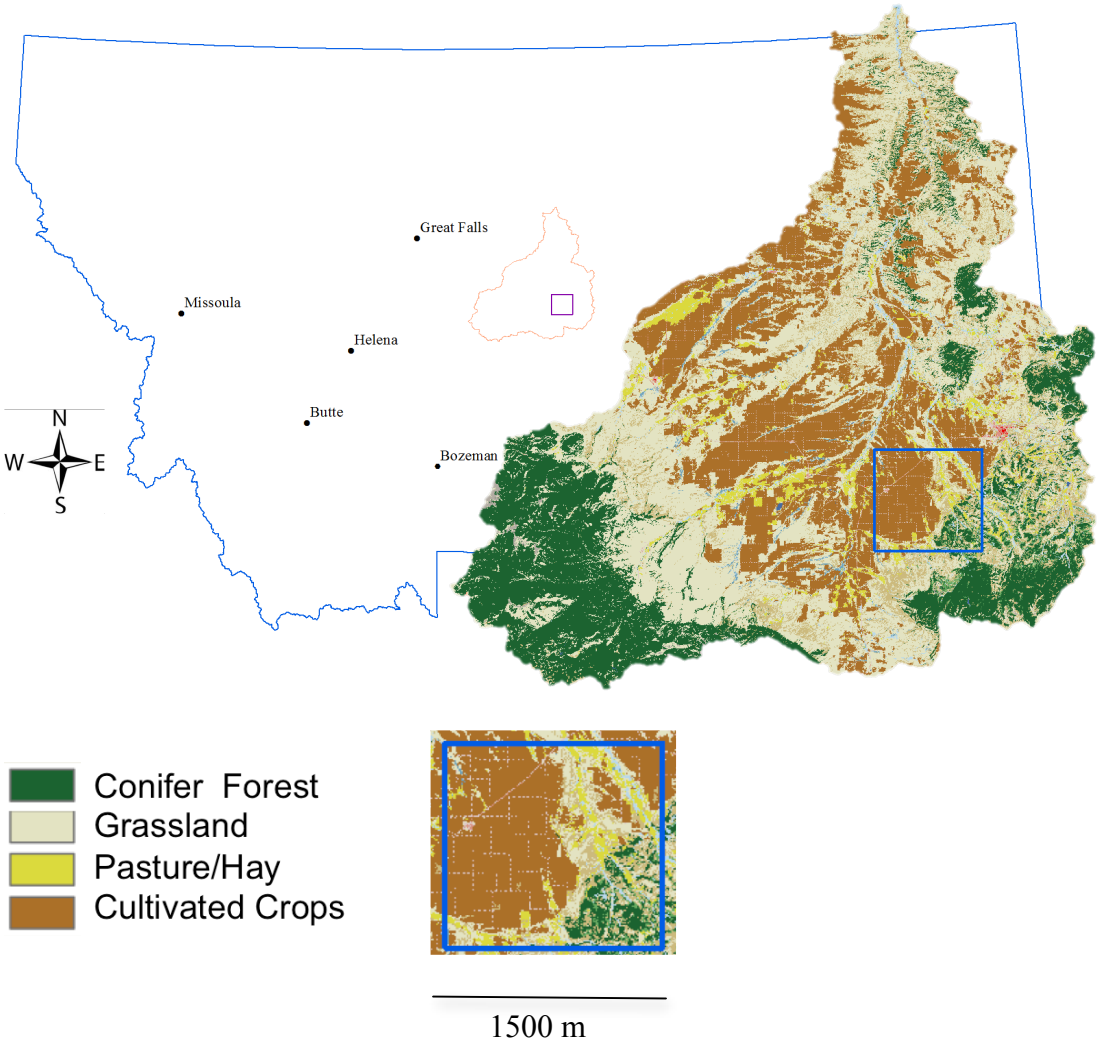


Figure 3.1: The Judith Watershed (inset) in the U.S. State of Montana. The lower center subplot represents a land cover classification of the study domain (highlighted in blue).

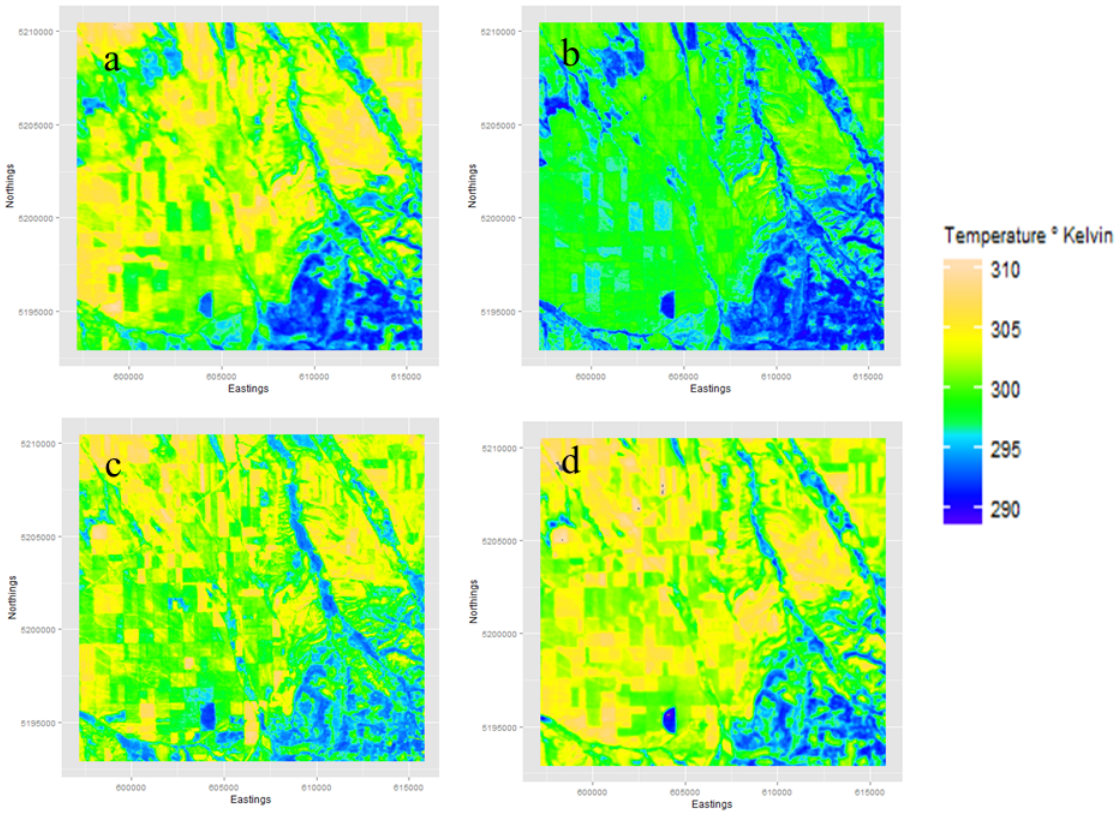


Figure 3.2. Land surface temperature in Kelvins, (a) Landsat TM mean LST August 7, 2011. (b) Landsat ETM+ LST July 30, 2011(c) Landsat ETM+ LST July 3, 2013. (d) LST from Landsat TIRS on July 27, 2013.

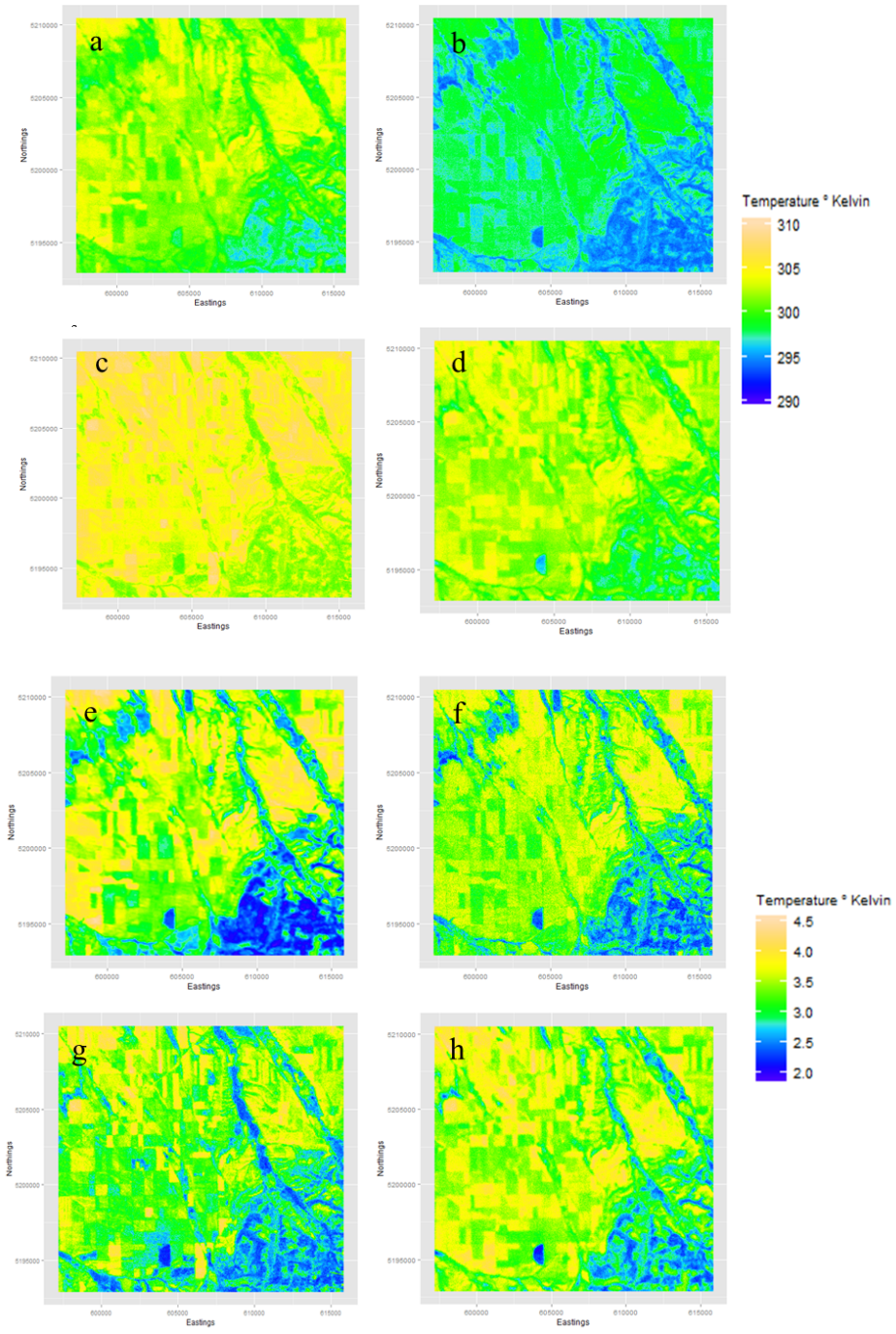


Figure 3.3. Mean and variance of LST layers created through Monte Carlo simulation of the parameters of MODTRAN. Mean images are shown on the left and variances on the right. (a) and (e) Landsat TM mean LST and variance of LST layers respectively, for August 7, 2011. (b) and (f) Landsat ETM+ July 30, 2011. (c) and (g) Landsat ETM+ July 3, 2013. (d) and (h) Landsat TIRS data from July 27, 2013.

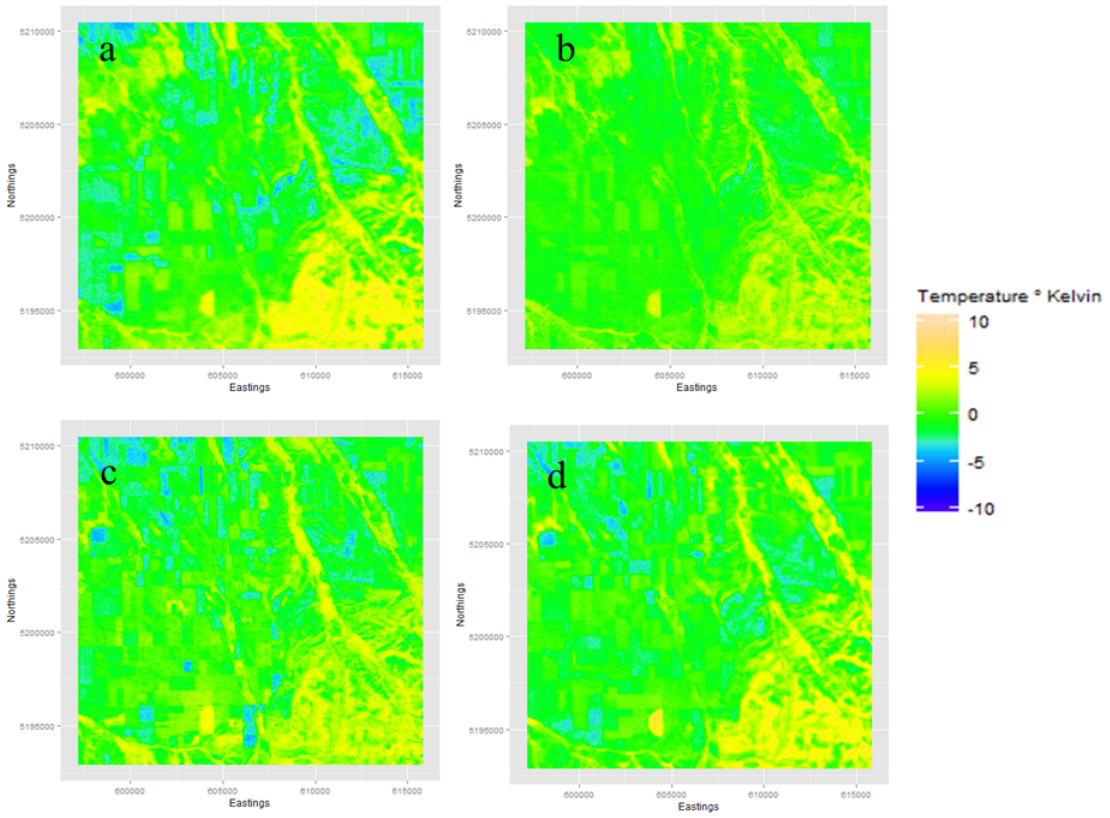


Figure 3.4. (a) Image differences in LST created from date specific adjustments and mean LST from Monte Carlo simulation of parameters for Landsat TM DOY 219 2011. (b) Image differences in LST created from date specific adjustments and mean LST from Monte Carlo simulation of parameters for Landsat ETM+ 211, 2011. (c) Image differences in LST created from date specific adjustments and mean LST from Monte Carlo simulation of parameters for Landsat ETM+ 184 2013. (d) Image differences in LST created from date specific adjustments and mean LST from Monte Carlo simulation of parameters for Landsat TIRS on DOY 208 2013.

Table 3.1. Data Attributes

| Landsat Thermal data | | | | |
|---|---|---|---|---|
| **Satellite Name** | **Band Number** | **Wavelength (micrometers)** | **Sampled Resolution** | **Pixel Resolution** |
| Landsat-5 TM | 6 | 10.40-12.50 | 120m | 30m |
| Landsat-7 ETM+ | 6 | 10.31-12.36 | 60m | 30m |
| Landsat-8 TIRS | 10 | 10.6-11.19 | 100m | 30m |

Table 3.2. Data Table

| **Sensor** | **DOY** | **Date** | **Year** | **K1** | **K2** |
|---|---|---|---|---|---|
| **TM** | 219 | 7-Aug | 2011 | 607.76 | 1260.56 |
| **ETM+** | 211 | 30-Jul | 2011 | 666.09 | 1282.71 |
| **ETM+** | 184 | 3-Jul | 2013 | 666.09 | 1282.71 |
| **L8** | 208 | 27-Jul | 2013 | 774.89 | 1321.08 |

Table 3.3. Variances in Degrees Kelvin

| Sensor | DOY | Total Variance | Variance of LST | Percent Variance from MODTRAN | Random Variance |
|---|---|---|---|---|---|
| TM | 219 | 61.1 | 4.42 | 7.23 | 56.68 |
| ETM+ | 211 | 7.19 | 1.94 | 9.61 | 5.25 |
| ETM+ | 184 | 33.7 | 3.24 | 26.98 | 30.46 |
| TIRS | 208 | 40.1 | 3.56 | 8.88 | 36.54 |

Acknowledgements

The Montana Institute on Ecosystems provided financial assistance. PCS acknowledges funding from the National Science Foundation (‘Scaling ecosystem function: Novel Approaches from MaxEnt and Multiresolution’, Division of Biological Infrastructure #1021095), the State of Montana and the U.S. Geological Survey.

# References


1. Barsi JA, Barker JL, Schott JR (2003) An atmospheric correction parameter calculator for a single thermal band earth-sensing instrument. Geosci. Remote Sens. Symp. 2003. IGARSS'03. Proceedings. 2003 IEEE Int. IEEE, pp 3014–3016

2. Barsi JA, Hook SJ, Palluconi FD, et al. (2006) Landsat TM and ETM+ thermal band calibration. SPIE Opt. Photonics. International Society for Optics and Photonics, p 62960F–62960F

3. Chander G, Markham BL, Helder DL (2009) Summary of current radiometric calibration coefficients for Landsat MSS, TM, ETM+, and EO-1 ALI sensors. Remote Sens Environ 113:893–903. doi: 10.1016/j.rse.2009.01.007

4. Cohen WB, Goward SN (2004) Landsat's role in ecological applications of remote sensing. Bioscience 54:535–545.

5. Coll, César, et al. "Validation of Landsat-7/ETM+ thermal-band calibration and atmospheric correction with ground-based measurements." Geoscience and Remote Sensing, IEEE Transactions on 48.1 (2010): 547-555.

6. Hill TC, Quaife T, Williams M (2011) A data assimilation method for using low-resolution Earth observation data in heterogeneous ecosystems. J Geophys Res 116:D08117. doi: 10.1029/2010JD015268

7. Irish RR (2000) Landsat 7 science data users handbook. Natl Aeronaut Sp Adm Rep 415–430.

8. Jarvis, P. G. "Scaling processes and problems." Plant, Cell & Environment18.10 (1995): 1079-1089.

9. Kerr JT, Ostrovsky M (2003) From space to species: ecological applications for remote sensing. Trends Ecol Evol 18:299–305.

10. Prieto-Blanco, Ana, et al. "Satellite-driven modelling of net primary productivity (NPP): theoretical analysis." Remote Sensing of Environment 113.1 (2009): 137-147.

11. Quattrochi DA, Luvall JC (2004) Thermal Remote Sensing in Land Surface Processing. Taylor & Francis

12. Stoy PC, Williams M, Disney M, et al. (2009) Upscaling as ecological information transfer: a simple framework with application to Arctic ecosystem carbon exchange. Landsc Ecol 24:971–986. doi: 10.1007/s10980-009-9367-3

13. Tan B, Masek JG, Wolfe R, et al. (2013) Improved forest change detection with terrain illumination corrected Landsat images. Remote Sens Environ 136:469–483.

# CHAPTER FOUR

## CONCLUSION

Determining the scale of change in this research proved difficult due to two reasons. Firstly, the scaling up of ecosystem functional scale to the data scale of Landsat data lost the detail needed to determine the transitions of expanding bog features in inland Alaska site. Additionally, the number of samples of ground data available for validation of bog feature classes was too small to adequately inform the Random Forest classification. However the analysis on scaling Landsat data provided incite for future research on applying multi-resolution scaling methods. Additionally, the work on uncertainty of Landsat data provides strong evidence on the minimal added uncertainty of the MODTRAN atmospheric correction method. One can feel confident that applying these atmospheric translations provides much benefit, which outweigh the additional variability posed by the translation. Methods for quantifying uncertainty associated a Landsat data derivative products are also provided by this analysis.

# REFERENCES CITED


1. Akansu, A.N. & Haddad, P.R., 2000. *Multiresolution signal decomposition:transforms, subbands, and wavelets*, Academic Press.

2. Anthony, K. W., Zimov, S. A., Grosse, G., Jones, M. C., Anthony, P. M., Chapin III, F. S., ... & Frolking, S. (2014). A shift of thermokarst lakes from carbon sources to sinks during the Holocene epoch. *Nature*.

3. Asner, Gregory P., Jonathan MO Scurlock, and Jeffrey A Hicke. "Global synthesis of leaf area index observations: implications for ecological and remote sensing studies." Global Ecology and Biogeography 12.3 (2003): 191-205.

4. Barsi JA, Barker JL, Schott JR (2003) An atmospheric correction parameter calculator for a single thermal band earth-sensing instrument. Geosci. Remote Sens. Symp. 2003. IGARSS'03. Proceedings. 2003 IEEE Int. IEEE, pp 3014–3016

5. Barsi JA, Hook SJ, Palluconi FD (2006) Landsat TM and ETM+ thermal band calibration. SPIE Opt. Photonics. International Society for Optics and Photonics, p 62960F–62960F

6. Bauer, I.E. & Vitt, D.H., 2011. Peatland dynamics in a complex landscape: Development of a fen-bog complex in the Sporadic Discontinuous Permafrost zone of northern Alberta, Canada. *Boreas*, 40(4), pp.714–726.

7. Bivand, Roger and Lewin-Koh, Nicholas, 2014. maptools: Tools for reading and handling spatial objects. R package version 0.8-30.

8. Bonan, G.B., 2002. *Ecological climatology: concepts and applications*, Cambridge University Press.

9. Breiman, Leo. "Random forests." *Machine learning* 45.1 (2001): 5-32.

10. Chapin, F. S., Sturm, M., Serreze, M. C., McFadden, J. P., Key, J. R., Lloyd, A. H., ... & Welker, J. M. (2005). Role of land-surface changes in Arctic summer warming. *science*, *310*(5748), 657-660.

11. Chander, G. & Markham, B., 2003. Revised Landsat-5 TM Radiometric Calibration Procedures and Postcalibration Dynamic Ranges. , 41(11), pp.2674–2677.

12. Chander, G., Markham, B.L. & Helder, D.L., 2009. Summary of current radiometric calibration coefficients for Landsat MSS, TM, ETM+, and EO-1 ALI

sensors. *Remote Sensing of Environment*, 113(5), pp.893–903. Available at: http://linkinghub.elsevier.com/retrieve/pii/S0034425709000169 [Accessed March 1, 2012].

13. Chapin, F.S. et al., 2005. Role of land-surface changes in arctic summer warming. *Science (New York, N.Y.)*, 310(5748), pp.657–60. Available at: http://www.ncbi.nlm.nih.gov/pubmed/16179434 [Accessed March 17, 2012].

14. Chander G, Markham BL, Helder DL (2009) Summary of current radiometric calibration coefficients for Landsat MSS, TM, ETM+, and EO-1 ALI sensors. Remote Sens Environ 113:893–903. doi: 10.1016/j.rse.2009.01.007

15. Christensen, T. R., Ekberg, A., Ström, L., Mastepanov, M., Panikov, N., Öquist, M., ... & Oskarsson, H. (2003). Factors controlling large scale variations in methane emissions from wetlands. *Geophysical Research Letters*,*30*(7).

16. Christensen, T.R. et al., 2004. Thawing sub-arctic permafrost: Effects on vegetation and methane emissions. *Geophysical Research Letters*, 31, p.L04501.

17. Cohen WB, Goward SN (2004) Landsat's role in ecological applications of remote sensing. Bioscience 54:535–545.

18. Coll, César "Validation of Landsat-7/ETM+ thermal-band calibration and atmospheric correction with ground-based measurements." Geoscience and Remote Sensing, IEEE Transactions on 48.1 (2010): 547-555.

19. Cutler, D.R. et al., 2012. Random Forests for Classification in Ecology Published by : Ecological Society of America content in a trusted digital archive . We use information technology and tools to increase productivity and facilitate new forms of scholarship . For more informatio. *Ecology*, 88(11), pp.2783–2792.

20. Daubechies, I., 1992. *Ten lectures on wavelets*, SIAM.

21. Ferguson, C. R., Sheffield, J., Wood, E. F., & Gao, H. (2010). Quantifying uncertainty in a remote sensing-based estimate of evapotranspiration over continental USA. *International Journal of Remote Sensing*, *31*(14), 3821-3865.

22. Fisher, Jeremy Isaac, John F. Mustard, and Matthew A. Vadeboncoeur. "Green leaf phenology at Landsat resolution: Scaling from the field to the satellite."Remote sensing of environment 100.2 (2006): 265-279.

23. Forbes, Bruce C., MARC FAURIA, and Pentti Zetterberg. "Russian Arctic arming and 'greening'are closely tracked by tundra shrub willows." Global Change Biology 16.5 (2010): 1542-1554.

24. Gislason, P.O., Benediktsson, J.A. & Sveinsson, J.R., 2006. Random forests for land cover classification. *Pattern Recognition Letters*, 27(4), pp.294–300.

25. Grosse, G. et al., 2011. Vulnerability of high-latitude soil organic carbon in North America to disturbance. *Journal of Geophysical Research*, 116, pp.1–23. Available at: http://www.agu.org/pubs/crossref/2011/2010JG001507.shtml [Accessed October 28, 2012].

26. Hijams, Robert, 2014. raster: Geographic data analysis and modeling. R package version 2.3-0.

27. Hill TC, Quaife T, Williams M (2011) A data assimilation method for using low-resolution Earth observation data in heterogeneous ecosystems. J Geophys Res 116:D08117. doi: 10.1029/2010JD015268

28. Houborg, R., Soegaard, H. & Boegh, E., 2007. Combining vegetation index and model inversion methods for the extraction of key vegetation biophysical parameters using Terra and Aqua MODIS reflectance data. *Remote Sensing of Environment*, 106(1), pp.39–58.

29. Hu, Zhenglin, Shafiqul Islam, and Yizong Cheng. "Statistical characterization of remotely sensed soil moisture images." Remote Sensing of Environment 61.2 (1997): 310-318.

30. Huang, C., Goward, S. N., Masek, J. G., Gao, F., Vermote, E. F., Thomas, N., ... & Townshend, J. R. (2009). Development of time series stacks of Landsat images for reconstructing forest disturbance history. *International Journal of Digital Earth*, *2*(3), 195-218.

31. Hyyppä, J., Hyyppä, H., Inkinen, M., Engdahl, M., Linko, S., & Zhu, Y. H. (2000). Accuracy comparison of various remote sensing data sources in the retrieval of forest stand attributes. Forest Ecology and Management, 128(1), 109-120.

32. Irish, R.R., 2000. Landsat 7 science data users handbook. *National Aeronautics and Space Administration, Report*, pp.415–430

33. Jarvis, P. G. "Scaling processes and problems." Plant, Cell & Environment18.10 (1995): 1079-1089.

34. Johnston, C. E., Ewing, S. A., Harden, J. W., Varner, R. K., Wickland, K. P., Koch, J. C., & Jorgenson, M. T. (2014). Effect of permafrost thaw on CO2 and CH4 exchange in a western Alaska peatland chronosequence. *Environmental Research Letters*, *9*(8), 08500

35. Jorgenson, M. T., and T. E. Osterkamp. "Response of boreal ecosystems to varying modes of permafrost degradation." *Canadian Journal of Forest Research* 35.9 (2005): 2100-2111.

36. Kerr JT, Ostrovsky M (2003) From space to species: ecological applications for remote sensing. Trends Ecol Evol 18:299–305.

37. Kumar, P. & Foufoula-Georgiou, E., 1997. Wavelet Analysis for Geophysical Applications. *Reviews of Geophysics*, 35(4), pp.385–412.

38. Lillesand, T. M., Kiefer, R. W., & Chipman, J. W. (2004). Remote sensing and image interpretation (No. Ed. 5). John Wiley & Sons Ltd.

39. Long, J. (2014). *Assessing changes in spatial and temporal patterns of cropping sequences in northeast Montana*. Bozeman, Montana: Montana State University.

40. Markham, B. L., Storey, J. C., Williams, D. L., & Irons, J. R. (2004). Landsat sensor performance: history and current status. Geoscience and Remote Sensing, IEEE Transactions on, 42(12), 2691-2694.

41. Meentemeyer, V., & Box, E. O. (1987). Scale effects in landscape studies. InLandscape heterogeneity and disturbance (pp. 15-34). Springer New York.

42. Moritz, Richard E., Cecilia M. Bitz, and Eric J. Steig. "Dynamics of recent climate change in the Arctic." Science 297.5586 (2002): 1497-1502.

43. Prieto-Blanco, Ana, et al. "Satellite-driven modelling of net primary productivity (NPP): theoretical analysis." Remote Sensing of Environment 113.1 (2009): 137-147.

44. Quattrochi DA, Luvall JC (2004) Thermal Remote Sensing in Land Surface Processing. Taylor & Francis

45. Ripley, Brian D. "Spectral analysis and the analysis of pattern in plant communities." The Journal of Ecology (1978): 965-981.

46. Roy, D. P., et al. "Landsat-8: Science and product vision for terrestrial global change research." Remote Sensing of Environment 145 (2014): 154-172.

47. Stoy PC, Williams M, Disney M (2009) Upscaling as ecological information transfer: a simple framework with application to Arctic ecosystem carbon exchange. Landsc Ecol 24:971–986. doi: 10.1007/s10980-009-9367-3

48. Stumpf, R. P., & Pennock, J. R. (1989). Calibration of a general optical equation for remote sensing of suspended sediments in a moderately turbid estuary.Journal of Geophysical Research: Oceans (1978–2012), 94(C10), 14363-14371.

49. Tan B, Masek JG, Wolfe R (2013) Improved forest change detection with terrain illumination corrected Landsat images. Remote Sens Environ 136:469–483.

50. Turner D. P., Ritts W. D., Cohen W. B., Maeirsperger T. K., Gower S. T., Kirschbaum A. A., Running S. W., Zhao M. S., Wofsy S. C., Dunn A. L., Law B. E., Campbell J. L., Oechel W. C., Kwon H. J., Meyers T. P., Small E. E., Kurc S. A. and J. A. Gamon (2005), Site-level evaluation of satellite-based global terrestrial gross primary production and net primary production monitoring, Global Change Biology, 11(4): 666-684